J. Fluid Mech. (1995), *vol.* 293, *pp.* 269–303

A general theory for two-dimensional vortex interactions

By DAVID G. DRITSCHEL

Department of Applied Mathematics and Theoretical Physics, University of Cambridge, Silver Street, Cambridge CB3 9EW, UK

(Received 9 May 1994 and in revised form 28 October 1994)

A general theory for two-dimensional vortex interactions is developed from the observation that, under slowly changing external influences, an individual vortex evolves through a series of equilibrium states until such a state proves unstable. Once an unstable equilibrium state is reached, a relatively fast unsteady evolution ensues, typically involving another nearby vortex. During this fast unsteady evolution, a fraction of the original coherent circulation is lost to filamentary debris, and, remarkably, the flow reorganizes into a set of quasi-steady stable vortices.

The simplifying feature of the proposed theory is its use of adiabatic steadiness and marginal stability to determine the shapes and separation distance of vortices on the brink of an inelastic interaction. As a result, the parameter space for the inelastic interaction of nearby vortices is greatly reduced. In the case of two vortex patches, which is the focus of the present work, inelastic interactions depend only on a single parameter: the area ratio of the two vortices (taking the vorticity magnitude inside each to be equal). Without invoking adiabatic steadiness and marginal stability, one would have to contend with the additional parameters of vortex separation and shape, and the latter is actually an infinitude of parameters.

1. Introduction

In the absence of strong external forcing and excessive dissipation, two-dimensional flows tend to organize themselves into well-defined, well-separated vortices within a sea of quasi-passive filamentary debris (Brachet *et al.* 1988; Santangelo, Benzi & Legras 1989; McWilliams 1990; Dritschel 1993 and references therein). The vortices are the characteristic structures of two-dimensional flows and their interactions with each other, particularly their inelastic interactions, i.e. merger or straining out, partial or complete (Dritschel & Waugh 1992), determine the overall organization, distribution and characteristics of the flow.

This observation has motivated recent attempts to formulate a theory of 2D flows, specifically turbulence, that is based on inelastic interactions (Carnevale *et al.* 1991; Benzi *et al.* 1992). However, fresh evidence suggests that the picture is considerably more complex than was imagined. In particular, (i) the local binary interaction of two vortices seldomly leads to a single compound vortex (this is why 'vortex merger' is not an appropriate term – see Dritschel & Waugh 1992), and (ii) the inelastic interaction of two vortices depends on at least one other vortex to push them close enough together (Dritschel 1993; Dritschel & Zabusky 1995).

So far, these theories have used crude quantitative results for the inelastic interaction process. There is a debate on whether or not more accurate quantitative results are necessary. Does the decaying state of two-dimensional turbulence depend on more

elaborate vortex interactions besides the merging of like-signed vortices? It is argued here that it does. In any case, the proposed theories are not consistent with the only two-dimensional turbulence data at sufficiently high resolution to test them (Dritschel 1993).

The goal in the present paper is not to formulate a theory of two-dimensional turbulence – this is regarded as too difficult a task at the present moment (for reasons why, see Dritschel & Zabusky 1995). Rather, the goal is to formulate a theory for the specific inelastic interactions that constitute turbulence. The latter is itself a difficult task, and it is necessary to invoke some kind of simplifying principle.

This paper invokes the principle of 'adiabatic steadiness', which states that, between inelastic interactions, vortices evolve through a sequence of near-equilibrium states, these states being parametrically determined by the instantaneous local straining flow exerted by surrounding vortices, until which time the equilibrium state proves unstable. Thereafter, a rapid, unsteady motion ensues, this being the inelastic interaction itself.

This principal rests on the assumption that vortices are, in general, widely separated, as in the latter stages of decaying two-dimensional turbulence simulations. This implies that surrounding vortices modify the shape of a given vortex at a rate much slower than the intrinsic frequency of the vortex (proportional to its peak vorticity), except when two vortices get sufficiently close together to precipitate an inelastic interaction. Note that we do not require that the irrotational strain experienced by a given vortex be small, but rather than its rate of change be small. Two nearby vortices exert significant strain upon one another while more distant vortices exert considerably weaker strain.

In the present work, we study in detail the case of two unequal-sized, patch-like vortices having either equal vorticity or, with novelty, opposite vorticity. We examine their equilibrium states (in §3), making the approximation that the strain exerted by other, distant vortices on the pair in question is weak compared to the strain exerted by members of the pair on each other. That is, the shape of each vortex is determined by the local equilibrium of two isolated vortices a certain distance apart. Their separation distance is, however, controlled by surrounding vortices not explicitly modelled. Then, we examine (in §4) the linear stability of these equilibrium states to determine the critical separation distance which precipitates an inelastic interaction.

The remarkable fact is that the two constraints of adiabatic steadiness and marginal stability reduce the parameter space to just one parameter: the area ratio of the two vortices. Quantitative results for the transition from one state to another, as a function of the initial area ratio, are then obtained in §5 from a series of high-resolution 'contour surgery' calculations (Dritschel 1988*a*, 1989*a*). A common initial stage of instability is observed and linked to the destabilization of an elliptical vortex. The emergence of a coherent quasi-steady state is also observed, and the return to near steadiness (in the large) is found to occur by way of an intense filamentation of the vortices' boundaries. Some conclusions and ideas for future applications and extensions are offered in §6.

2. Adiabatic evolution

In this section, a single example illustrates the striking tendency for vortices to evolve adiabatically in the presence of slowly changing external straining. The example generalizes the one given by Legras & Dritschel (1993), who considered a single vortex (both a patch and a smooth profile) within a pure adverse shear growing linearly in time from zero to mimic the approach of two vortices initially far apart.

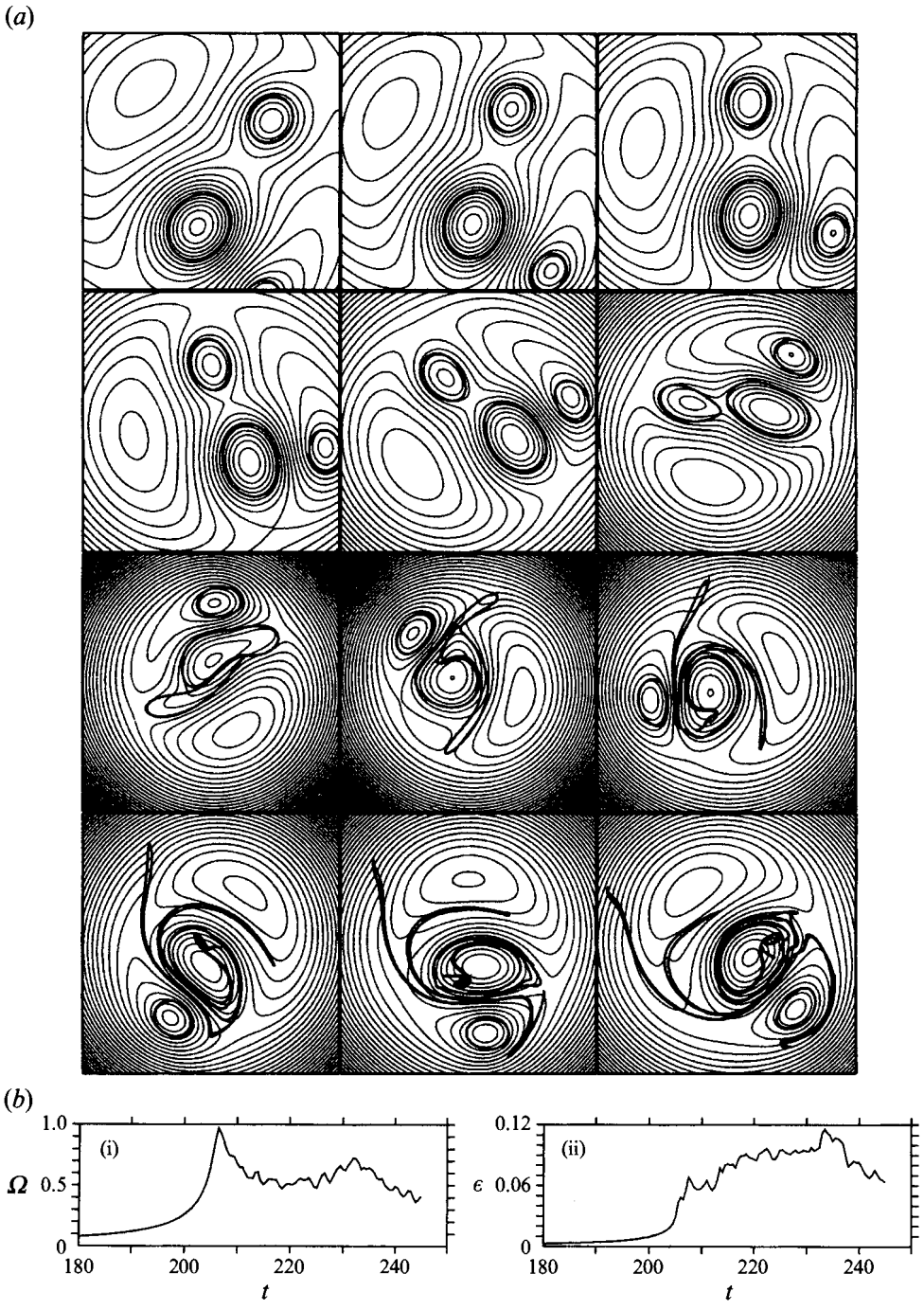

FIGURE 1. (*a*) The evolution of the three collapsing vortex patches. Contours of vorticity ω are shown in bold superposed on those of the streamfunction in a particular co-rotating frame of reference (see Appendix A). Time advances to the right and downwards in unit intervals (i.e. vortex half-rotation periods) starting at $t = 200$. (*b*) The background rotation rate Ω (i) and the dimensionless degree of unsteadiness ϵ (ii) versus time; Ω and ϵ are defined in Appendix A. ϵ is computed for the entire vorticity distribution, including the debris produced after the interaction, which is why it does not diminish significantly after the interaction.

In the example considered here, three distantly separated vortex patches are initially positioned in a configuration which would cause a corresponding set of point vortices to collapse to a point in finite time (Gröbli 1877; Aref 1979). For point vortices, the collapse initial conditions have zero measure (taking, say, the mean inter-centroid distance between the vortices to have a given value), but for vortex patches there is a finite probability that the vortices may get close enough to undergo an inelastic interaction.

The conditions for point vortex collapse are as follows: (i) given two like-signed vortices, of strengths κ_1 and κ_2, the third vortex must have strength $\kappa_3 = -\kappa_1\kappa_2/(\kappa_1+\kappa_2)$, which is opposite in sign to the other two, and (ii) the third vortex must lie along either of two arcs of a certain circle whose centre lies at the centroid of the two like-signed vortices (Aref 1979).

In the calculation to be illustrated, we consider three vortex patches, of vorticity magnitude 2π and areas π, $\pi/2$ and $\pi/3$. Initially, the two like-signed (positive) vortices are separated (centre-to-centre) by 20 units (i.e. 20 radii of the largest vortex patch). The third (negative) vortex is positioned on the collapse circle at the angle $\theta = -45°$. The collapse time for the corresponding point vortices is $t = t_c = 205.65$.

This and other calculations presented in this paper are performed using 'contour surgery', (Dritschel 1988*a*, 1989*a*), a refined contour dynamics (Zabusky, Hughes & Roberts 1979) algorithm with an automatic and well-tested method for removing fine-scale filamentary debris. In all calculations presented in this paper, filamentary debris are removed below the scale $\delta = 0.0009$. This level of 'surgery' corresponds to a maximum node separation of $\mu = 0.06$. The time step (of a fourth-order Runge–Kutta scheme) is here set to 0.05, half the maximum suggested value, for a high level of accuracy.

Figure 1(*a*) illustrates the evolution of the three vortex patches up to the time of collapse; contours of vorticity ω (bold) and streamfunction (in a particular rotating frame of reference – see Appendix A for details) ψ (light) are superposed to indicate the degree to which the vortices are in mutual equilibrium (figure 1*b* gives a quantitative measure, ϵ, proportional to the r.m.s. normal velocity). The slight, growing misalignment of the ω and ψ contours before the collapse time (around $t = 206$) is due almost entirely to the growing eccentricity of and the collapsing separation distance between the three vortices as they fall in toward each other. That is, some misalignment is necessary even to pass adiabatically from one near-equilibrium state to another (see also the discussion in Legras & Dritschel 1993). The actual degree to which the contours are aligned is significant, since the evolving vortex configuration is, by construction, unsteady. The three vortices fall in toward each other at an accelerated pace until the collision – here the inelastic interaction – takes place. Afterwards, the two principal coherent vortices re-adjust to a near equilibrium (as seen by the near correspondence of their ω and ψ contours). Remarkably, the transition from one near equilibrium state to another occurs on a vortex-rotation timescale (2 units of time).

3. Equilibrium states for two unequal vortex patches

We next examine the steadily co-rotating states for two unequal-area vortex patches having either the same (uniform) vorticity or opposite vorticity. Such a configuration is the simplest non-trivial configuration that one can consider. Moreover, vortex patches having equal vorticity magnitudes are arguably a good approximation to the types of vortices one would see after many inelastic interactions in turbulence (Dritschel & Waugh 1992; Dritschel 1993). This is simply because the most extreme levels of vorticity have the greatest chance of survival – peripheral vorticity is rendered

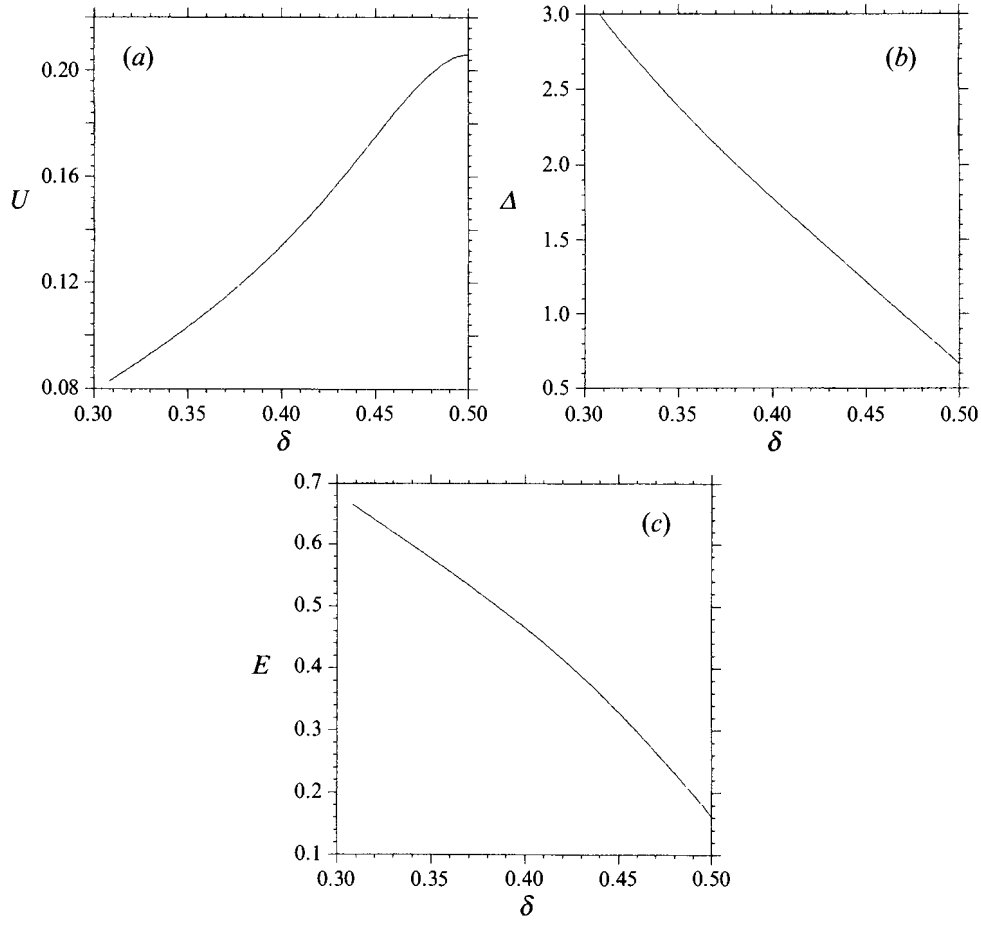

FIGURE 8. Properties of two equal-area opposite-signed equilibrium vortex patches: (*a*) the translation velocity U, (*b*) the distance between vortex centroids Δ and (*c*) the excess energy E as a function of the relative thickness δ. The linear impulse I satisfies $I = \pi\Delta$. The margin of stability is at $\delta = 0.472$.

(*d*) the excess energy E. Diagnostics for the special case, $\alpha = 1$, are shown in figure 8: in (*a*) the translation velocity U; in (*b*) the distance between vortex centroids Δ; and in (*c*) the excess energy E as a function of δ. (Note that, in the limit $\alpha \to 1$, the scaled rotation rate tends to $2U/\Delta$ while the scaled angular impulse tends to $-I\Delta/4$, where I is the linear impulse, i.e. $I = \int\int \omega(\boldsymbol{x})\, y \,\mathrm{d}x\,\mathrm{d}y$.) An additional curve is again drawn on the contour plots (in figure 7) to show the margin of instability; all solutions having greater δ (to the right of this curve) are unstable (see §4 below). Note that the marginal stability curve does not always pass through a simultaneous extremum of both J and E (taken as functions of δ, for fixed α) even though these extrema still coexist. This result casts doubt on the universality of Saffman's theory (Saffman 1992), previously supported in the case of like-signed vortices (further details are given below in §4).

Finally, the contour plots of J and E cannot be used to search for the possibility of inviscid transitions because different equilibria generally have different areas of positive and negative vorticity.

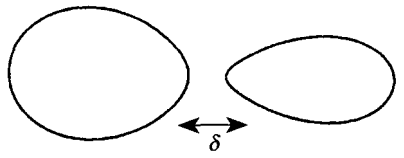

FIGURE 2. Schematic of the equilibrium state of two like-signed vortex patches.

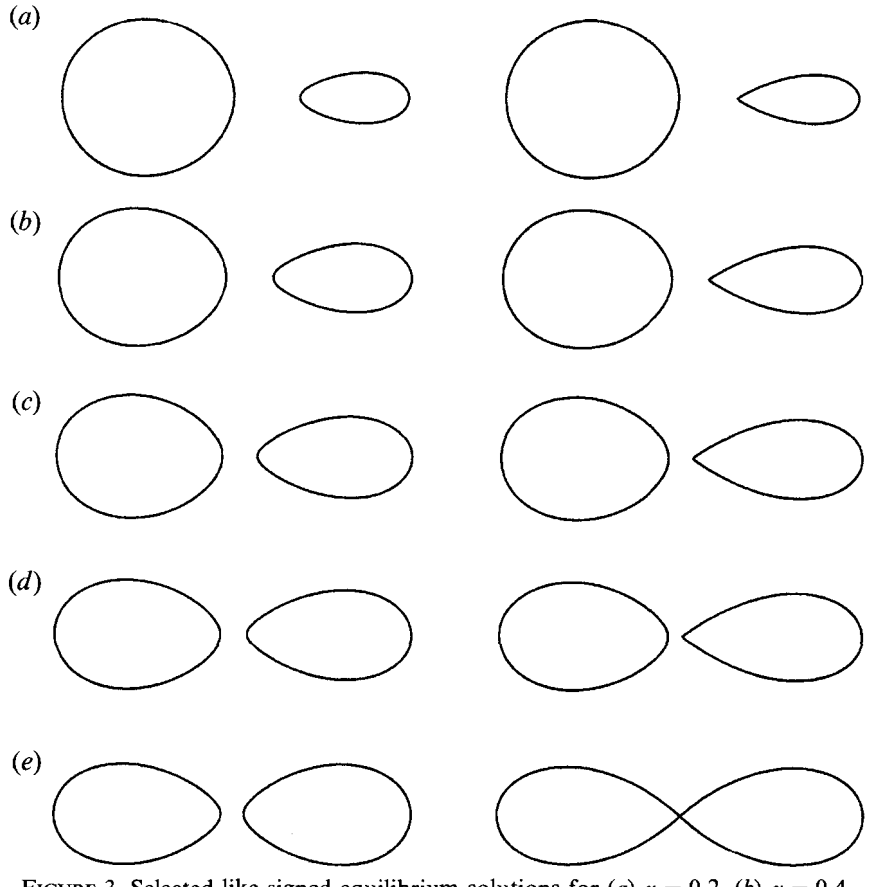

FIGURE 3. Selected like-signed equilibrium solutions for (*a*) $\alpha = 0.2$, (*b*) $\alpha = 0.4$, (*c*) $\alpha = 0.6$, (*d*) $\alpha = 0.8$ and (*e*) $\alpha = 1$.

and in (*d*) the 'excess energy' (see Dritschel 1989*a*), where

$$E = -\frac{1}{4\pi}\int\int\int\int \omega(\boldsymbol{x})\,\omega(\boldsymbol{x}')\log|\boldsymbol{x}-\boldsymbol{x}'|\,\mathrm{d}x\,\mathrm{d}y\,\mathrm{d}x'\,\mathrm{d}y'.$$

In the contour plots, an additional curve is drawn to indicate the margin of instability (all solutions with smaller δ to the left of this curve are unstable, according to the direct eigen-analysis of the next section). Note that this curve passes through a simultaneous extremum of both J and E (taken as functions of δ, for fixed α). The entire lower branch of the double-values $E(J)$ curve is unstable, in apparent agreement with the theory of Saffman (1992) (in particular, see Kamm 1987). But see the case for opposite-signed vortices below.

The contour plots of J and E also reveal that inviscid transitions, i.e. evolutionary transitions involving a negligible loss of filamentary debris (Dritschel 1985, 1986) are

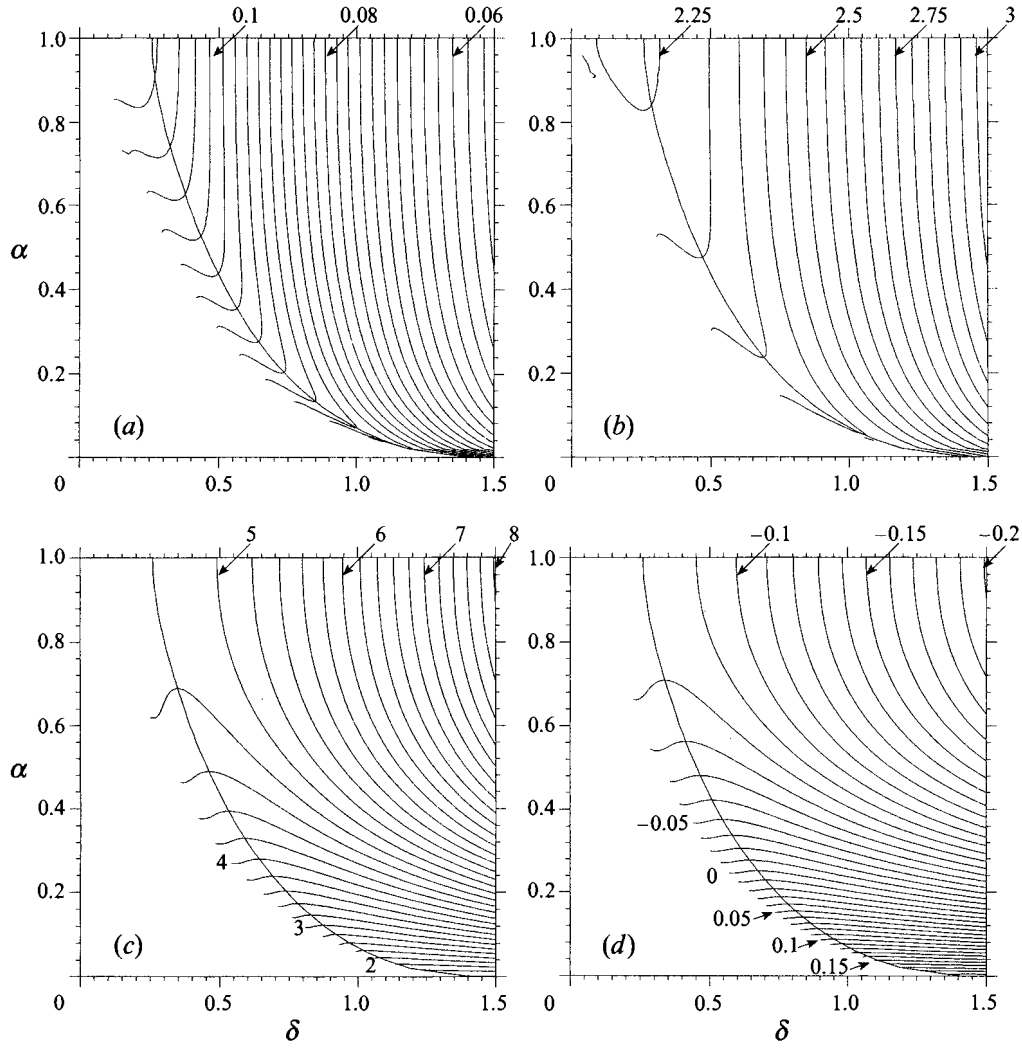

FIGURE 4. Contour maps of (*a*) the rotation rate Ω, (*b*) the distance between vortex centroids Δ, (*c*) the angular impulse J and (*d*) the excess energy E as a function of the gap δ and area ratio α for the like-signed equilibrium solutions. The additional curve indicates the margin of instability.

possible between all points (δ, α) and (δ', α') which have identical J and E (the circulation is the same for all states, by design). (Inviscid transitions also require that the symmetry of the final state be consistent with the symmetry of the initial one, as here.) The only sensible transitions are between unstable and stable states, and the unstable states are seen to lie just inside the marginal stability curve. This implies that transitions beginning from marginally unstable states – explored below in § 5 – will in general produce little filamentary debris.

3.2. *Opposite-vorticity equilibria*

For two vortices having opposite vorticity, it is difficulty to choose a distance measure that picks up the complete family of equilibria for all vortex area ratios. The one that has been found to work best, after many attempts, is the width of the smaller vortex divided by width of the entire configuration, this ratio of widths being denoted δ, with

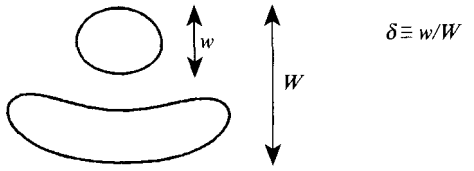

FIGURE 5. Schematic of the equilibrium state of two-opposite-signed vortex patches.

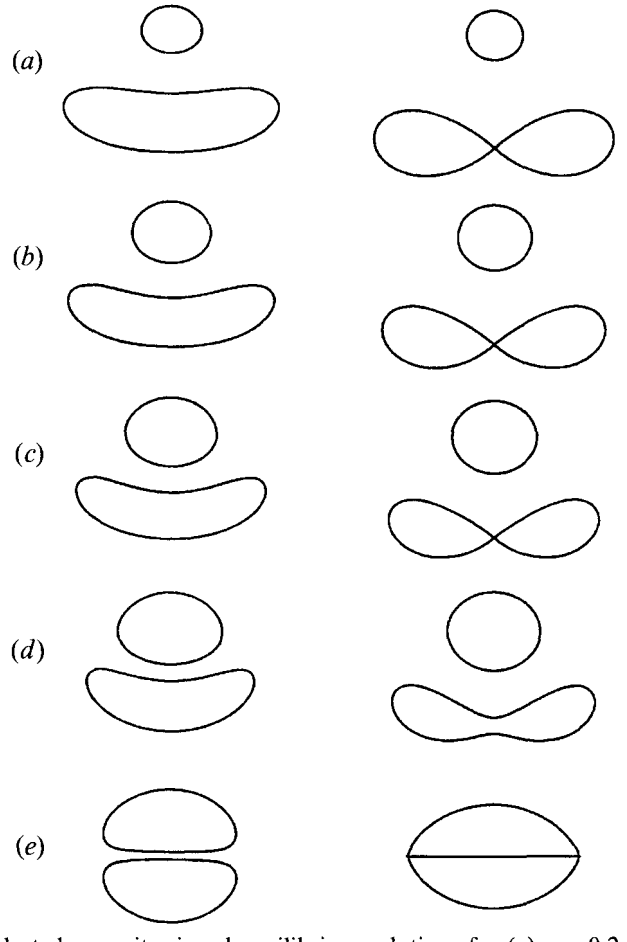

FIGURE 6. Selected opposite-signed equilibrium solutions for (*a*) $\alpha = 0.2$, (*b*) $\alpha = 0.4$, (*c*) $\alpha = 0.6$, (*d*) $\alpha = 0.8$ and (*e*) $\alpha = 1$.

the widths calculated along the symmetry axis – see the schematic in figure 5. The sum of the vortex areas is again taken to be π, which implies that equilibria with different area ratios have different circulations, unlike in the previous case of like-signed vortices.

The numerical scheme used to calculate the equilibria is slightly modified to take care of the fact that $\Omega \to 0$ as $\alpha \to 1$, i.e. in the limit of equal area, the two vortices do not rotate; they translate. (These equal-area states were formerly calculated by Pierrehumbert 1980). The criterion for accepting a solution is thus stiffened to $2\pi|\Omega'|(1+\alpha)/(1-a) < 10^{-7}$. In the limit $\alpha \to 1$, $\Omega(1+\alpha)/(1-\alpha) \to 2U/\Delta$, where U is the translation rate of the vortices and Δ is their inter-centroid separation.

Figure 6 shows two members of each family of equilibrium solutions for $\alpha = 0.2, 0.4,$

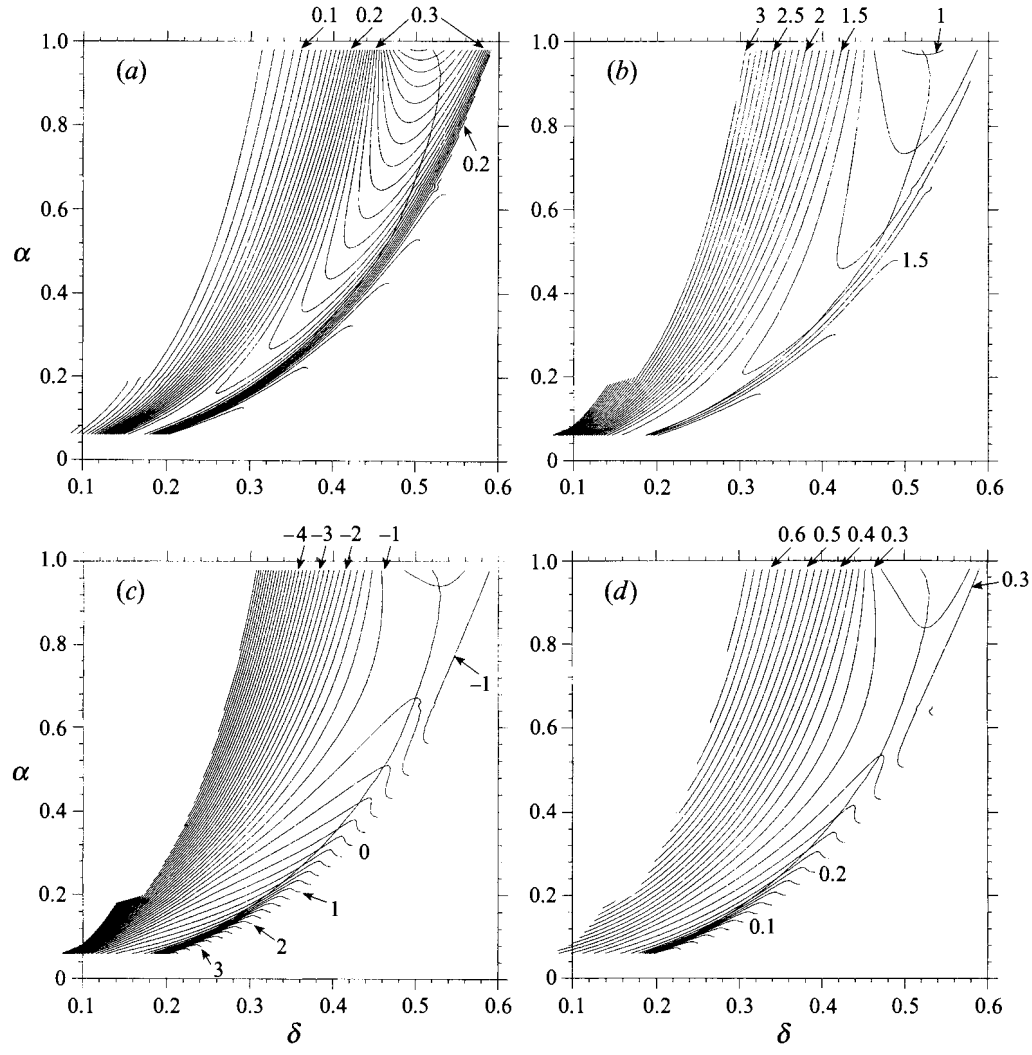

FIGURE 7. Contour maps of (*a*) the scaled rotation rate $\Omega(1+\alpha)/(1-\alpha)$, (*b*) the distance between vortex centroids Δ, (*c*) the scaled angular impulse $J(1-\alpha)/(1+\alpha)$ and (*d*) the excess energy E as a function of the relative thickness of the smaller vortex δ and area ratio α for the opposite-signed equilibrium solutions. The additional curve indicates the margin of instability.

0.6, 0.8 and 1; the solutions on the left are the marginally unstable ones, while those on the right are the limiting ones (or, when $\alpha = 0.8$, the furthest state that could be reached). There are two significant features to be noted. First, the equal-area equilibria look very different from the unequal-area equilibria and have a totally different limiting form. Second, the limiting states for unequal vortices exhibit a splitting of the larger vortex, even for small area ratios. It is conjectured that this behaviour continues all the way to $\alpha = 0$ where the solution joins to the limiting state for two *equal*-vorticity vortices (see figure 3*e*).

Figure 7, as a counterpart to figure 4, shows various basic diagnostics for the opposite-signed equilibrium solutions as a function of δ and α (excluding the special case $\alpha = 1$); in (*a*) the scaled-system rotation rate $\Omega(1+\alpha)/(1-\alpha)$; in (*b*) the distance between vortex centroids Δ; in (*c*) the scaled angular impulse $J(1-\alpha)/(1+\alpha)$; and in

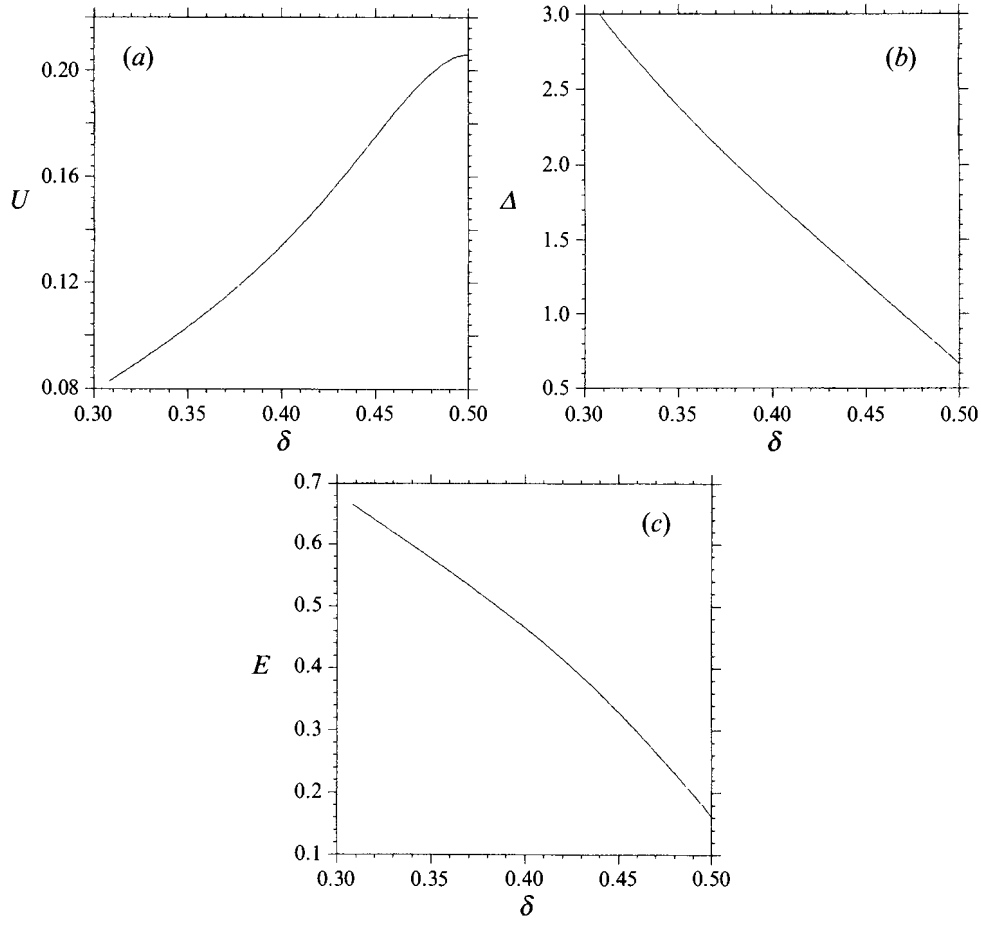

FIGURE 8. Properties of two equal-area opposite-signed equilibrium vortex patches: (*a*) the translation velocity U, (*b*) the distance between vortex centroids Δ and (*c*) the excess energy E as a function of the relative thickness δ. The linear impulse I satisfies $I = \pi\Delta$. The margin of stability is at $\delta = 0.472$.

(*d*) the excess energy E. Diagnostics for the special case, $\alpha = 1$, are shown in figure 8: in (*a*) the translation velocity U; in (*b*) the distance between vortex centroids Δ; and in (*c*) the excess energy E as a function of δ. (Note that, in the limit $\alpha \to 1$, the scaled rotation rate tends to $2U/\Delta$ while the scaled angular impulse tends to $-I\Delta/4$, where I is the linear impulse, i.e. $I = \int\int \omega(\boldsymbol{x})\, y \,\mathrm{d}x\,\mathrm{d}y$.) An additional curve is again drawn on the contour plots (in figure 7) to show the margin of instability; all solutions having greater δ (to the right of this curve) are unstable (see §4 below). Note that the marginal stability curve does not always pass through a simultaneous extremum of both J and E (taken as functions of δ, for fixed α) even though these extrema still coexist. This result casts doubt on the universality of Saffman's theory (Saffman 1992), previously supported in the case of like-signed vortices (further details are given below in §4).

Finally, the contour plots of J and E cannot be used to search for the possibility of inviscid transitions because different equilibria generally have different areas of positive and negative vorticity.

4. Linear stability

To determine when two vortices in near equilibrium may be expected to undergo an inelastic interaction, the equilibrium states are subjected to a full linear stability analysis, in which the equilibrium boundaries are displaced by arbitrary infinitesimal disturbances. Details of the method may be found in Appendix B.

The linear stability results for like-signed vortex patches are given in figure 9, which shows the growth rate σ_r (the real part of σ) as a function of the vortex gap δ and the area ratio α. The growth rate monotonically increases for $\delta < \delta_m(\alpha)$, the marginal stability boundary. The instability in all cases takes the form of 'an exchange of stability', in which the imaginary part of σ falls to zero (like $(\delta-\delta_m)^{1/2}$) on the approach to marginal stability and remains zero for all $\delta < \delta_m$. The marginal stability curve coincides with the extrema of the angular impulse J and excess energy E when considered a function of δ, as noted above in §3.

Figure 10 shows the corresponding results for opposite-signed vortex patches. The growth rate is generally non-monotonic due to the presence of multiple modes of instability (see figure 11). The first-encountered instability with increasing δ is of the exchange-of-stability type, yet, curiously, it corresponds to the joint extremum of angular impulse and excess energy only for $\alpha \gtrsim 0.7$. That is, the argument, based on Kelvin's variational principle (Saffman 1992 and references therein), that the margin of stability can be decided from the $E(J)$ curve alone (for an exchange-type mode of instability and regarding α as a fixed parameter) does not always work. For opposite-signed vortices, there are unstable states on both sides of this curve. It is notable that the topology of the $E(J)$ curve does not change with α, despite the saddle-type region in the contour plots for E and J. An extended discussion may be found in Dritschel (1985, §11) and in Kamm (1987).

5. Nonlinear evolution and transitions

We next examine the nonlinear evolution of the marginally unstable states, first to verify that the marginally unstable states do precipitate inelastic interactions, secondly to see what general features characterize the unsteady stage of evolution, and thirdly to quantify the transition between one coherent state and another.

The contour surgery algorithm is again used (with the parameter settings unchanged from §2). The calculations shown exhibit great complexity, requiring one to four hours at a calculation rate close to 1 Gflop, and to control this complexity, 'surgery' or the removal of fine-scale filamentary structures is essential. The surgery also facilitates the quantification of the coherent remnants of the evolution (regions of vorticity can both fuse and separate), allowing one to quantify a transition simply by tracking, as a function of time, the area contained within the largest contours.

Calculations were performed for the marginally unstable equilibrium states having area ratios $\alpha = 0.1, 0.2, \ldots, 1$. Any instability was allowed to develop from numerical noise (i.e. from the error in approximating a continuous curve by a finite number of nodes). The vorticity within each patch is scaled up to 2π so that 2 units of time corresponds to the rotation period of an isolated circular vortex. A frame of reference rotating at the equilibrium rotation rate is employed. A few representative calculations are illustrated next, first for equal-vorticity interactions then for opposite-vorticity interactions.

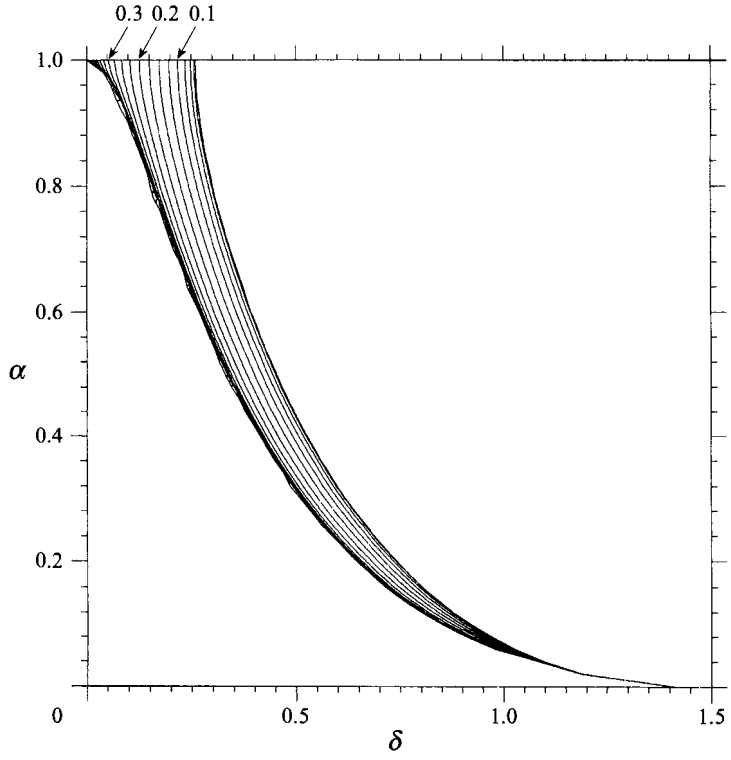

FIGURE 9. The growth rate σ_r plotted as a function of δ and α for the like-signed equilibrium states. The contour interval is 0.025 (recall that the vorticity is unity within the vortices).

5.1. *Equal-vorticity interactions*

Figure 12 shows the case $\alpha = 0.1$. The finite-amplitude instability is evident by $t = 16$ (third frame): a thin tongue of vorticity is drawn off the smaller vortex and subsequently wrapped around the larger. The transition is essentially complete 12 units of time later, with the smaller vortex shrinking by about a third in area and the larger vortex remaining unchanged. In a previous study (Dritschel & Waugh 1992), this type of inelastic interaction was called 'partial straining-out'. Note that the final coherent state is close to being in equilibrium.

Figure 13 shows the case $\alpha = 0.3$. We see the same initial stage of the evolution as in the previous case. Here, however, more circulation is contained within the filament encircling the larger vortex, and around $t = 24$ (fifth frame), we see the commencement of a strong interaction between the filament and the larger vortex, inducing substantial filamentation (Dritschel 1988*b*) and culminating in a loss of coherent circulation from the larger vortex (around 2%). Here, we have an example of an inelastic interaction that leaves two smaller vortices! Note again that the final coherent state is close to being in equilibrium.

Figure 14 shows the case $\alpha = 0.6$. Again we see the same initial stage of evolution, though the filament being drawn off the smaller vortex begins to strongly interact with the larger vortex before it detaches. More circulation is drawn from the smaller vortex than in previous cases, and this trend continues with increasing α up to $\alpha = 1$. This case is of special significance because the larger vortex neither shrinks nor grows significantly in circulation, despite severe agitation of its boundary. The evolution falls on the

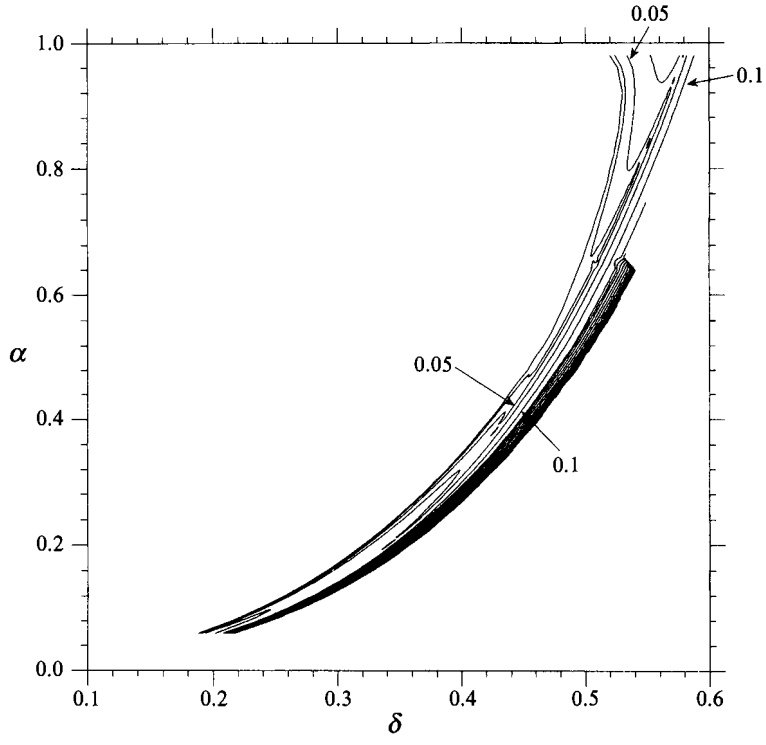

FIGURE 10. The growth rate σ_r plotted as a function of δ and α for the opposite-signed equilibrium states. The contour interval is 0.025.

boundary of the 'partial straining-out' and 'partial merger' regimes of inelastic interactions. Again, the final coherent state is close to being in equilibrium.

Figure 15 shows the case $\alpha = 0.9$. Once again we see the same initial stage of evolution, only with an earlier interaction between the filament and the larger vortex. One might say that the filament expulsion and its joining with the larger vortex occur almost simultaneously. This case begins to resemble (up to $t = 12$, the second frame) the classical picture of vortex merger that is based on symmetric vortex interactions, yet, by $t = 16$, we see a rapid departure from the classical picture: the vortices only partially merge before separating into two large coherent pieces. Here, the larger vortex grows significantly (by 20%) while the smaller vortex shrinks (by 70%) in a way characteristic of this regime of 'partial merger'. Once again, the final coherent state is close to being in equilibrium.

Several common evolutionary features are apparent. First, the instability begins in the same way, via the eruption of a tongue of vorticity from the inward-pointing nose of the smaller vortex. This behaviour is closely similar to that exhibited by a steady elliptical vortex patch in a linear background straining flow (i.e. a combination of pure deformation and pure rotation; for specific results, see equation (36) and figure 14 of Dritschel 1990). The first mode of instability encountered upon parametrically increasing the strain rate has three-fold symmetry (i.e. the disturbance function is given by $\eta = A\cos 3\theta + B\sin 3\theta$). (Increasing the strain rate is analogous to decreasing the vortex separation in the calculations just described.) This is significant since the nonlinear evolution of a mode 3 instability (see figure 22 of Dritschel 1990), has precisely the initial form seen here. And one can see this once more in the mode 3

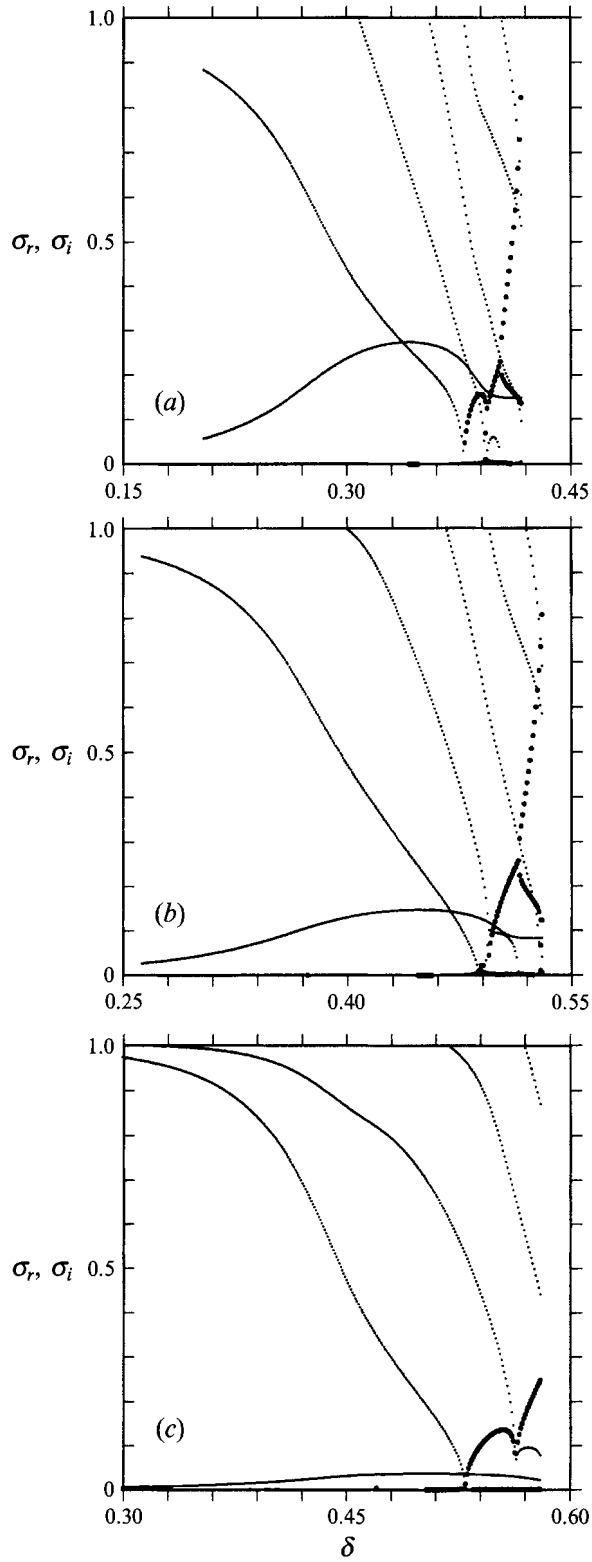

FIGURE 11. The frequency σ_i (small dots) and the growth rate σ_r (larger dots) plotted as a function of δ for (*a*) $\alpha = 0.3$, (*b*) $\alpha = 0.6$ and (*c*) $\alpha = 0.9$ for opposite-signed equilibrium states.

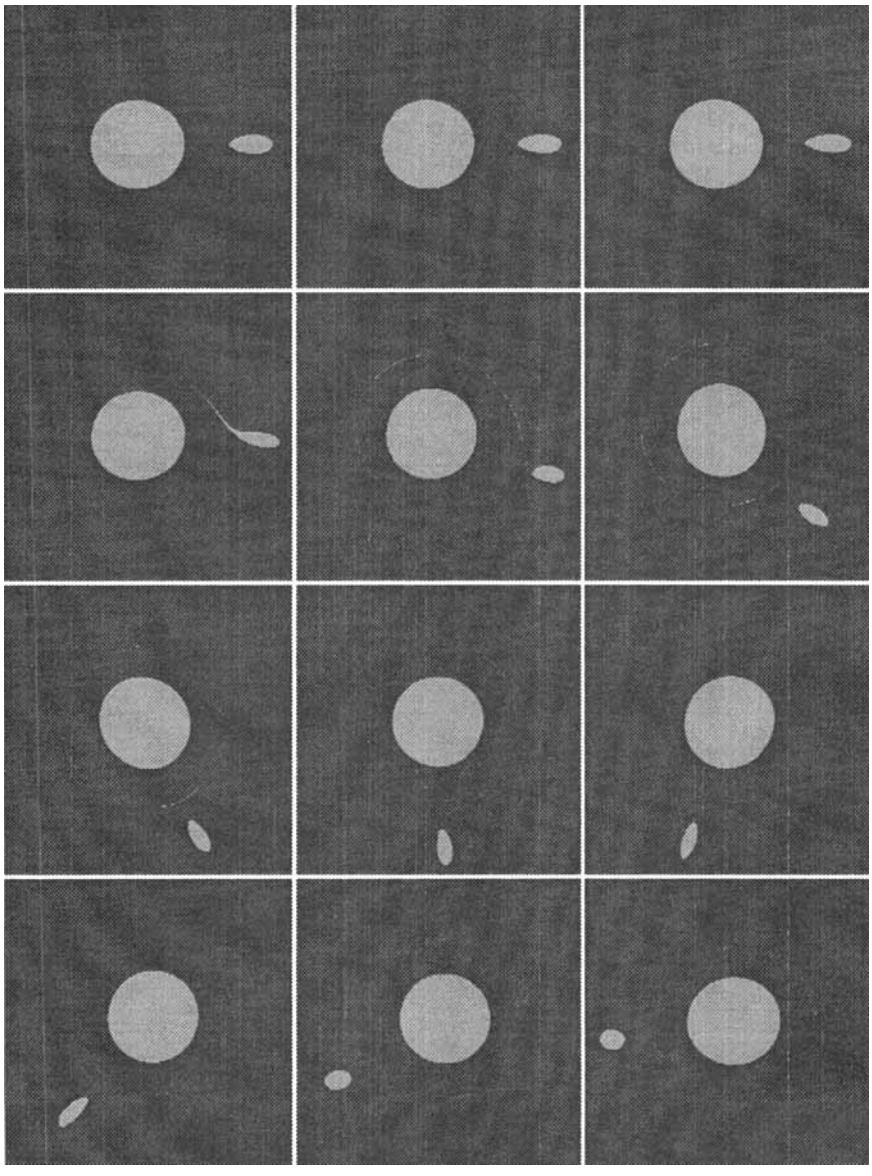

FIGURE 12. Evolution of the marginally unstable like-signed equilibrium state for $\alpha = 0.1$. Time advances to the right and downwards. The initial condition is shown in the upper left frame. Four units of time separate successive frames in this and subsequent figures, except for the first two frames. The gap of time between the first two frames depends on the level of noise and is therefore not particularly meaningful (it is, however, normally 12 units for like-signed interactions and between 32 and 56 units for opposite-signed ones).

instability of a freely rotating Kirchhoff elliptical vortex (see figures 12 and 13 of Dritschel 1986).

The second notable evolutionary feature is the remarkable return of the flow to a near equilibrium. It appears that this return to near equilibrium occurs through the homogenization of the enormous filamentary complexity riding on the vortex boundaries after the initial strong interaction of the two vortices (e.g. see figure 16 for a close-up of the calculation for $\alpha = 0.9$ at $t = 40$). An explanation for this cannot be

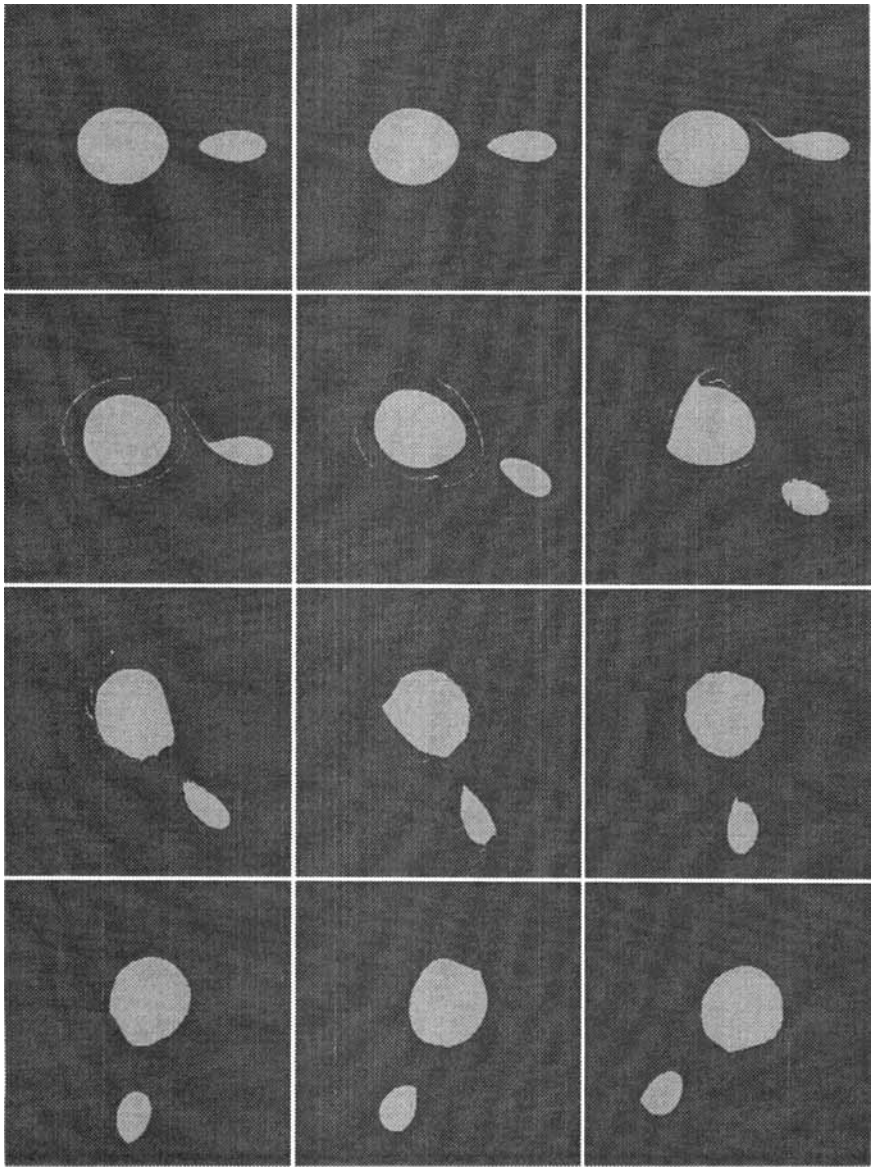

FIGURE 13. As in figure 12, but for $\alpha = 0.3$.

put forward at the present time; it is clear from figure 16 that numerical resolution effects can hardly be the cause.

We now return to an examination of the numerical calculations and consider the equal-area case, $\alpha = 1$, in figure 17. Here, we see a qualitative change in the initial evolution: the two vortices merge with little filamentary debris into one compound vortex, which subsequently undergoes an instability (starting at $t = 16$) very similar to that of a mode 4 disturbance to a 6:1 ellipse (see figure 12 of Dritschel 1986). The tips of the filamentary tongues roll up into small satellite vortices, leading to three coherent vortices.

But now contrast this with the slightly asymmetric case $\alpha = 0.99$, shown in figure 18. The initial evolution is like the symmetric case in the previous figure, but the

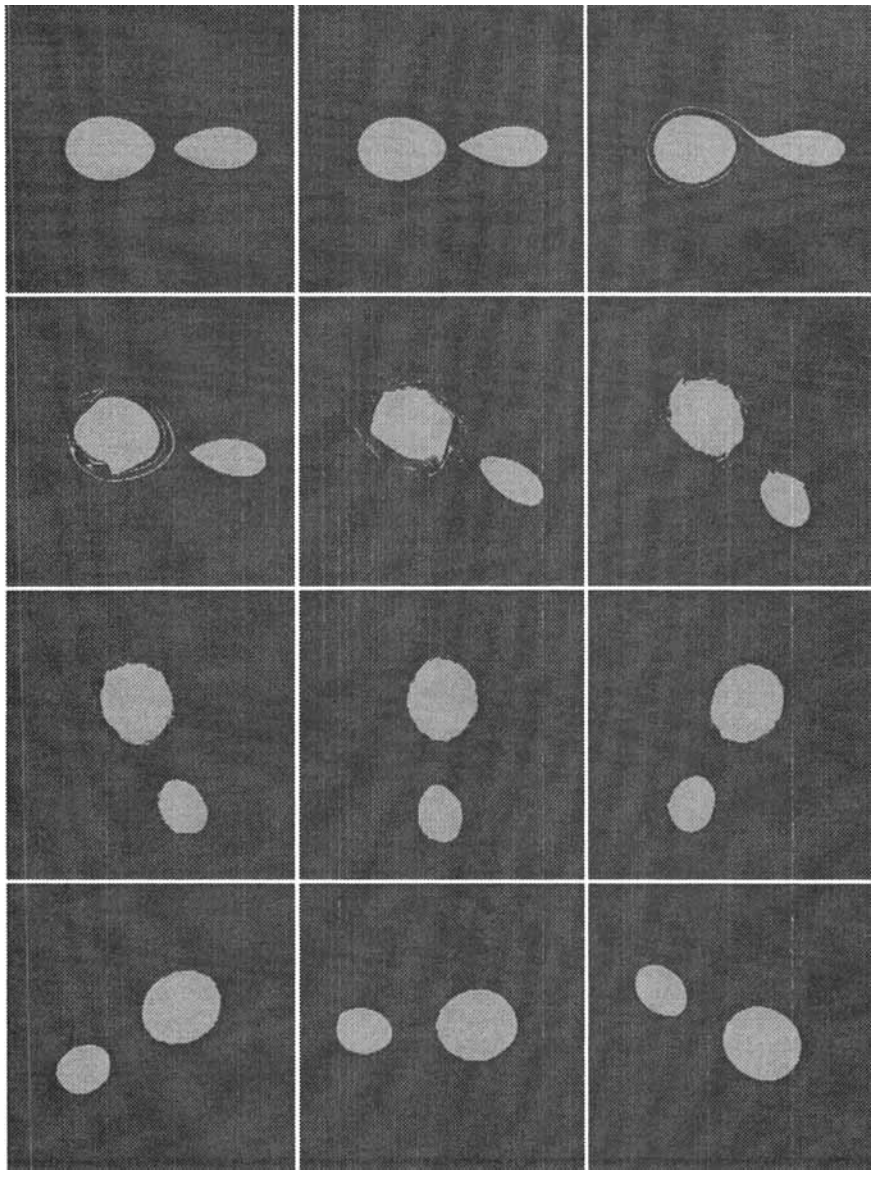

FIGURE 14. As in figure 12, but for $\alpha = 0.6$.

subsequent instability of the compound vortex is very different: it is instead like the instability of a mode-3 disturbance to a 6:1 ellipse (see figure 12 of Dritschel 1986). The fact is that the mode-3 disturbance is the first to destabilize with increasing aspect ratio, though at a 6 to 1 aspect ratio both modes 3 and 4 have comparable growth rates. The conclusion here is that the case $\alpha = 1$ is exceptional: in the presence of a weak external flow, three-fold disturbances will almost always dominate four-fold ones in the interaction of two vortices, even if they be of equal area (which is itself extremely unlikely).

The results for like-signed vortices have been quantified by computing the time evolution of the areas of the four largest contours in each calculation; see figure 19 for two examples: $\alpha = 0.3$ and $\alpha = 0.9$. After a short transition period, on the order of a

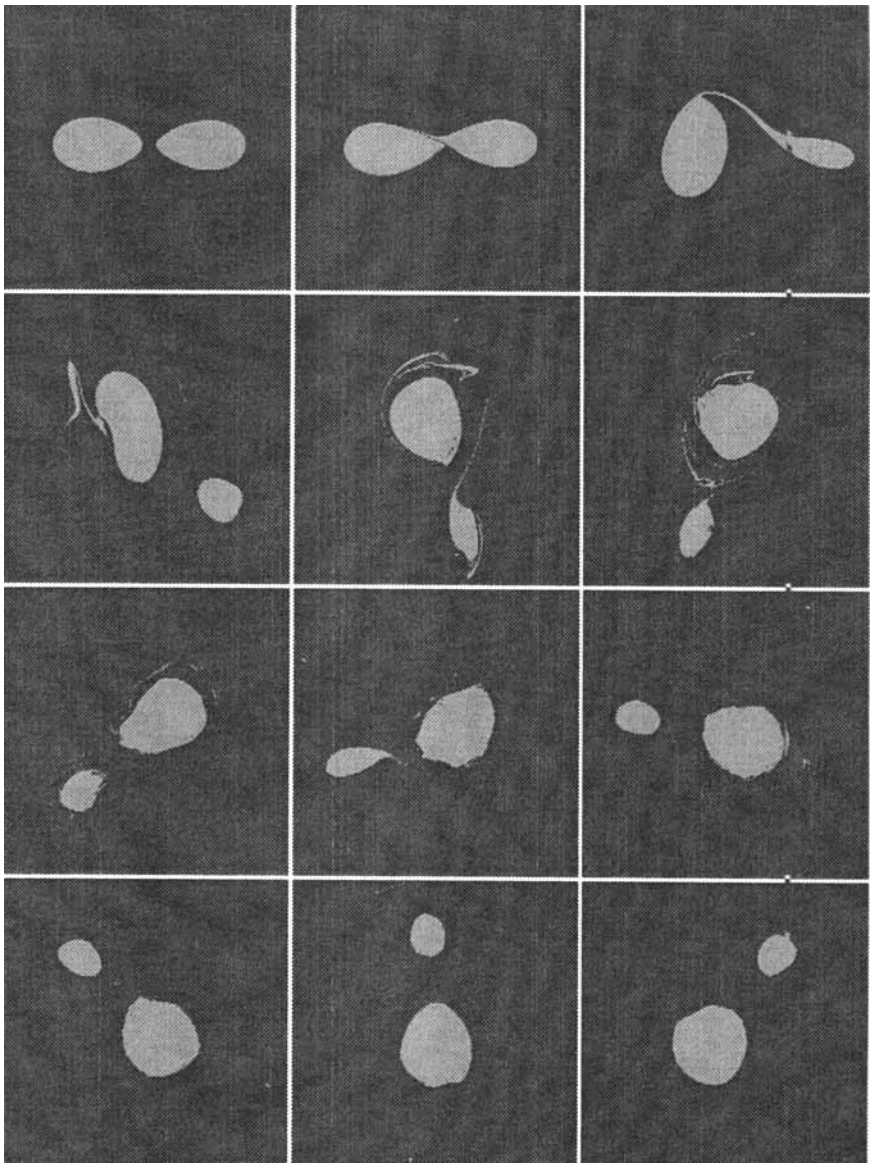

FIGURE 15. As in figure 12, but for $\alpha = 0.9$.

vortex rotation period, a remarkably invariant signal of two dominant quasi-steady vortices is re-established. The invariance of this signal permits one to draw a clear picture of the transition from one coherent flow state to another. This picture is displayed in figures 20(*a*) and 20(*b*). See also table 1. Figure 20(*a*) shows, as a function of the initial vortex area ratio α, the initial vortex areas divided by π as the solid curves, the final vortex areas divided by π as the large squares, the final vortex area ratio as the small diamonds, and the 'efficiency' of the transition, i.e. the ratio of the final to initial area within the coherent vortices, as the plusses. Note that the small vortex always gets smaller, while the larger vortex gets larger only for area ratios $\alpha \gtrsim 0.6$. This leads to the interesting result that the final vortex area ratio is always less than 0.5. The

FIGURE 16. Close-up view of figure 15 at $t = 40$ (eighth frame).

amount of filamentary debris increases with increasing α, reaching 21 % of the initial area for nearly equal vortices. Figure 20(*b*) shows the initial distance between vortex centres, Δ_i, before the transition takes place. Note that Δ_i is nearly independent of α, giving a simple criterion for the onset of an inelastic interaction: $\Delta^2 \lesssim 1.7\mathscr{A}$, or more precisely, $\Delta^2 \lesssim [1.609 + 0.253(1-\alpha)^2 \pm 0.004]\mathscr{A}$, where $\mathscr{A}$ is the total area of the two vortices.

The solid circles plotted in Figure 20(*b*) show the critical distance for the onset of an inelastic interaction for two initially circular vortices that was obtained in a previous work (Dritschel & Waugh 1992). This distance was computed by finding a corresponding equilibrium state of the same angular impulse and area ratio, and using the distance between these equilibrium vortices. In fact, this transformed distance differs remarkably little, never more than 0.5 %, from the original distance between the circular vortices (thus the distortion of the equilibrium states from a circular state contributes negligibly to the angular impulse). What we do see here is that the circular initial conditions overestimate the critical distance for the onset of an inelastic interaction between vortices in mutual equilibrium by 8–10 %.

Dritschel & Waugh (1992) also obtained results for the interaction of vortices within the critical distance. If we map the results of the present paper to their regime diagram, particularly the critical distance for an inelastic interaction (of two equilibrium vortices), by associating an equivalent circular-vortex initial condition having identical angular impulse, we find that the critical distance curves crosses all four regimes of

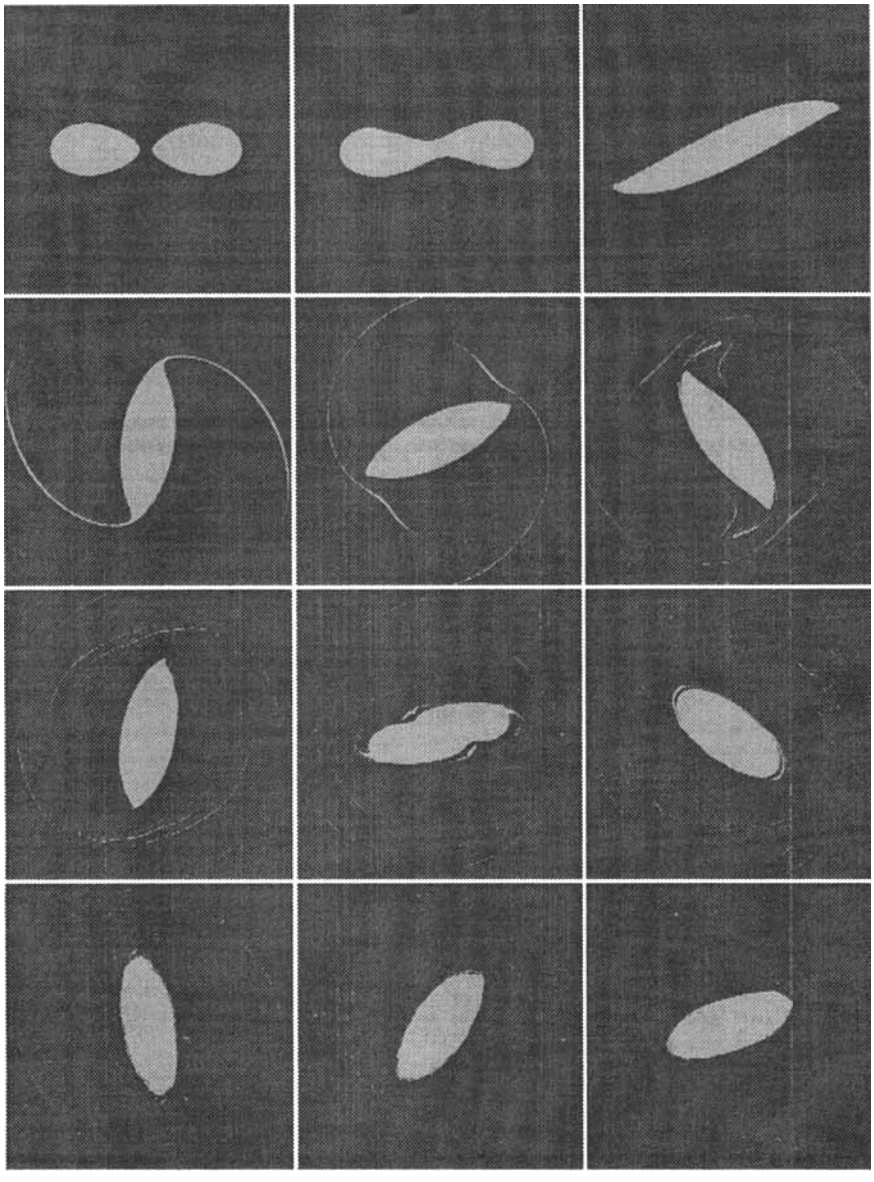

FIGURE 17. As in figure 12, but for $\alpha = 1$.

inelastic interaction – see figure 21. In the present work, radius ratios less than $\sqrt{0.1} \approx 0.3$ were not examined, so no comment can be made about the crossover from complete straining out to partial straining out at $R_2/R_1 \approx 0.18$. However, data are available for the crossover from partial straining out to partial merger: in figure 21, this is seen to occur at $R_2/R_1 \approx 0.59$, whereas the actually observed crossover occurs at $R_2/R_1 \approx \sqrt{0.6} \approx 0.77$. The final crossover from partial to complete merger at $R_2/R_1 \approx 0.98$ is approximately the same in both models. The conclusion is that the results for circular vortices are only qualitatively similar to those for equilibrium vortices.

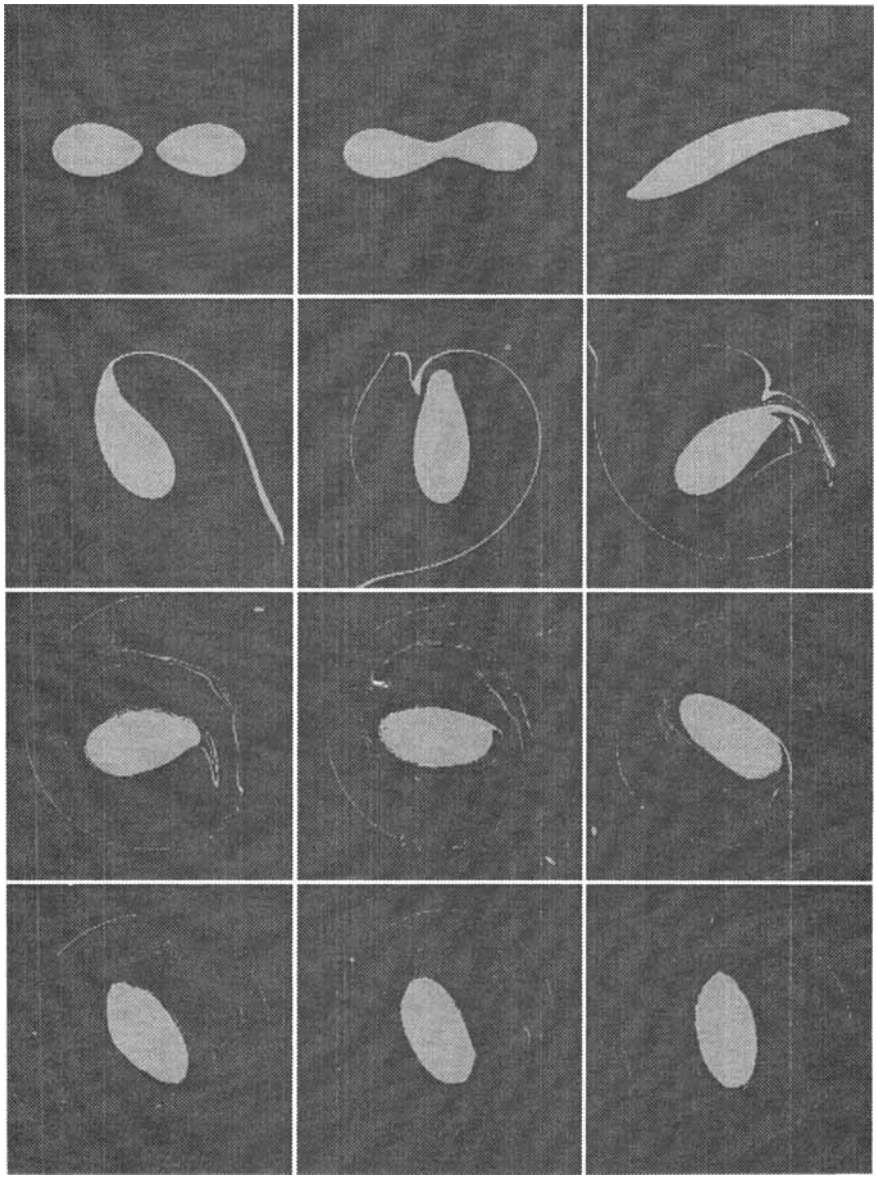

FIGURE 18. As in figure 12, but for $\alpha = 0.99$.

5.2. *Opposite-vorticity interactions*

Next we turn to opposite-signed vortex interactions. The possibility of inelastic interaction involving opposite-signed vortices seems not to have been considered previously, and indeed there are some surprises in store. Three representative calculations are illustrated. Figure 22 shows the case $\alpha = 0.1$. The instability commences in a way analogous to the like-signed cases above. A thin tongue of vorticity is drawn off the larger (but more eccentric) vortex, but, in contrast to the like-signed case, the tip of the thin filament rolls up into a small vortex (which is hard to see in the present example). Of course, with opposite-signed vortices, the two original vortices cannot merge. What we see, rather is the partial breakup of the larger vortex.

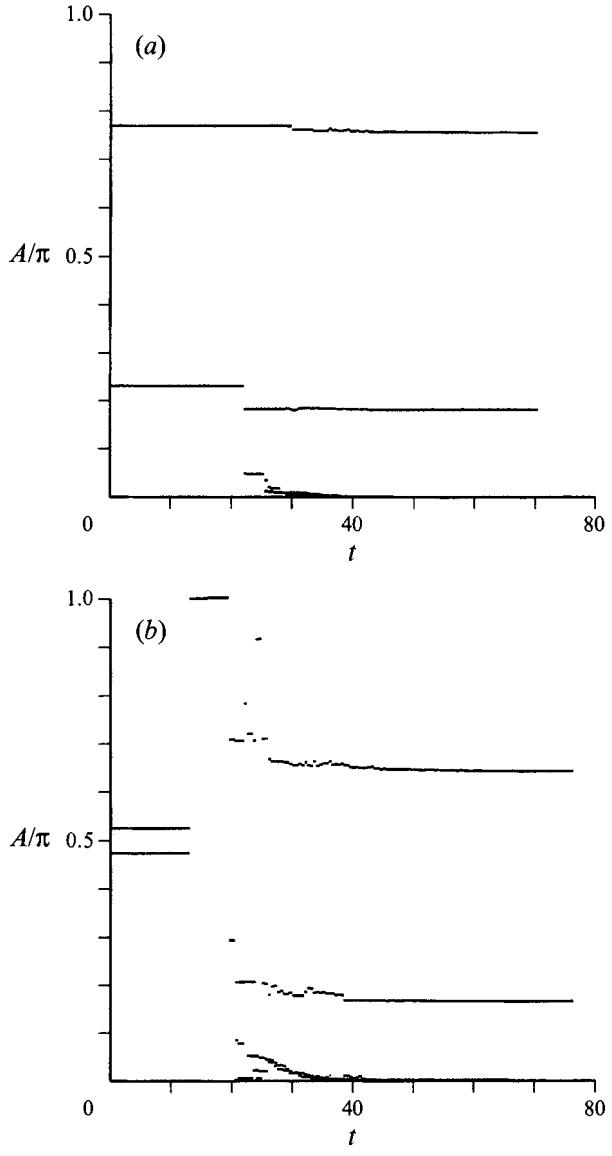

FIGURE 19. The areas (divided by π) of the four largest contours versus time for (*a*) $\alpha = 0.3$ and (*b*) $\alpha = 0.9$ (for like-signed vortices).

Figure 23 shows the case $\alpha = 0.7$. We see the same initial stage of the interaction and the formation of a larger satellite vortex from the roll-up of the tongue originally drawn from the larger vortex. We see, additionally, the expulsion of a tongue of vorticity from the smaller vortex, apparently by the close passage of the satellite vortex. This second tongue forms in a way exactly analogous to the first tongue; the smaller vortex of the original two momentarily looks like the larger of a mismatched dipole when the satellite vortex passes by. Note that the flow relaxes to a near-equilibrium state (if one excludes the small satellite vortex).

Figure 24 shows the perfectly matched dipole case, $\alpha = 1$. Despite the symmetry of the initial state, an asymmetric instability develops, and the evolution proceeds like in the previous cases, albeit with the production of a larger satellite vortex and with the

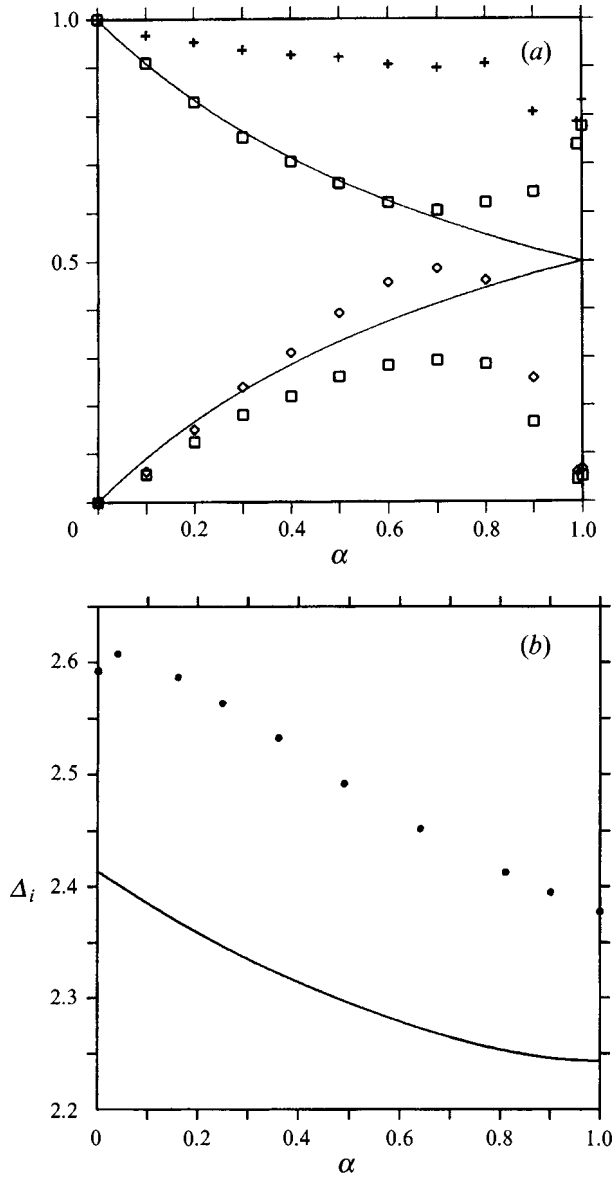

FIGURE 20. (*a*) Transition summary diagram for the inelastic interaction of two like-signed vortex patches. As a function of the initial vortex area ratio α, the solid curves give the initial vortex areas divided by π, the squares give the final vortex areas divided by π, the diamonds give the final vortex area ratio, and the crosses give the efficiency (the ratio of the final and initial area within the two principal vortices). (*b*) The distance between vortex centres before the transition; the solid circles correspond to the results found by Dritschel & Waugh (1992) for circular initial conditions (see text for explanation). See also table 1.

removal of a larger tongue of vorticity from the smaller original vortex. Again, the flow consisting of the two primary vortices relaxes to a near-equilibrium state. This relaxation occurs in the same way as for like-signed vortices, namely via the homogenization of the filaments riding on the vortex boundaries. The final state is less steady here because the degree of filamentation is significantly less for opposite-signed vortex interactions than for like-signed ones.

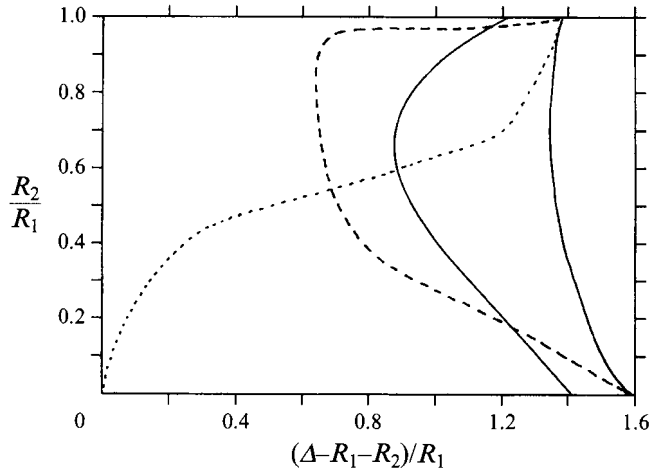

FIGURE 21. Figure adapted from Dritschel & Waugh (1992) showing the regimes of vortex interactions for two initially circular vortices. Vortex radius ratio, R_2/R_1, is shown versus the dimensionless gap between vortices, $(\Delta - R_1 - R_2)/R_1$. The rightmost solid curve shows the boundary between elastic and inelastic interactions, the short-dashed curve separates interactions which result in a net circulation gain of the larger vortex (above curve, merger) from those which result in no circulation gain (straining out), and the long-dashed curve separates complete merger or straining out (left) from partial merger or straining out (right). The new result shown in this figure is the left-hand solid curve, which corresponds to the boundary between elastic and inelastic interactions for the non-circular equilibrium states of the present paper.

α_i	Δ_i/L	α_f	Δ_f/L
0.10	2.385	0.0635	2.765
0.20	2.359	0.1499	2.735
0.30	2.335	0.2386	2.872
0.40	2.314	0.3105	3.006
0.50	2.295	0.3925	3.077
0.60	2.279	0.4561	3.178
0.70	2.265	0.4851	3.238
0.80	2.254	0.4605	3.148
0.90	2.246	0.2568	3.019
0.99	2.243	0.0624	1.497

TABLE 1. Equal-vorticity vortex transition properties: shown are the vortex area ratios and intercentroid distances before (subscript i) and after (subscript f) an inelastic interaction. Δ_f was computed from a time average over five to ten vortex rotation periods late in each calculation. Here, $L \equiv (\mathscr{A}/\pi)^{1/2}$, $\mathscr{A}$ being the total coherent area within the two principal vortices.

The quantitative results for opposite-signed vortices are given in figure 25 and table 2, which shows the properties of the transition from the initial coherent state, consisting of two vortices, to the final one, consisting of three. The format for this figure is similar to its counterpart for like-signed vortices, figure 20, except that in (*a*) there is an additional set of small squares for the area (divided by π) of the small satellite vortex torn from the larger of the original two. Note that both the smaller and the larger vortices decrease in area through the transition, and that the final area ratio remains equal to or slightly greater than the initial area ratio, in stark contrast to the results found for like-signed vortices. The amount of filamentary debris, however,

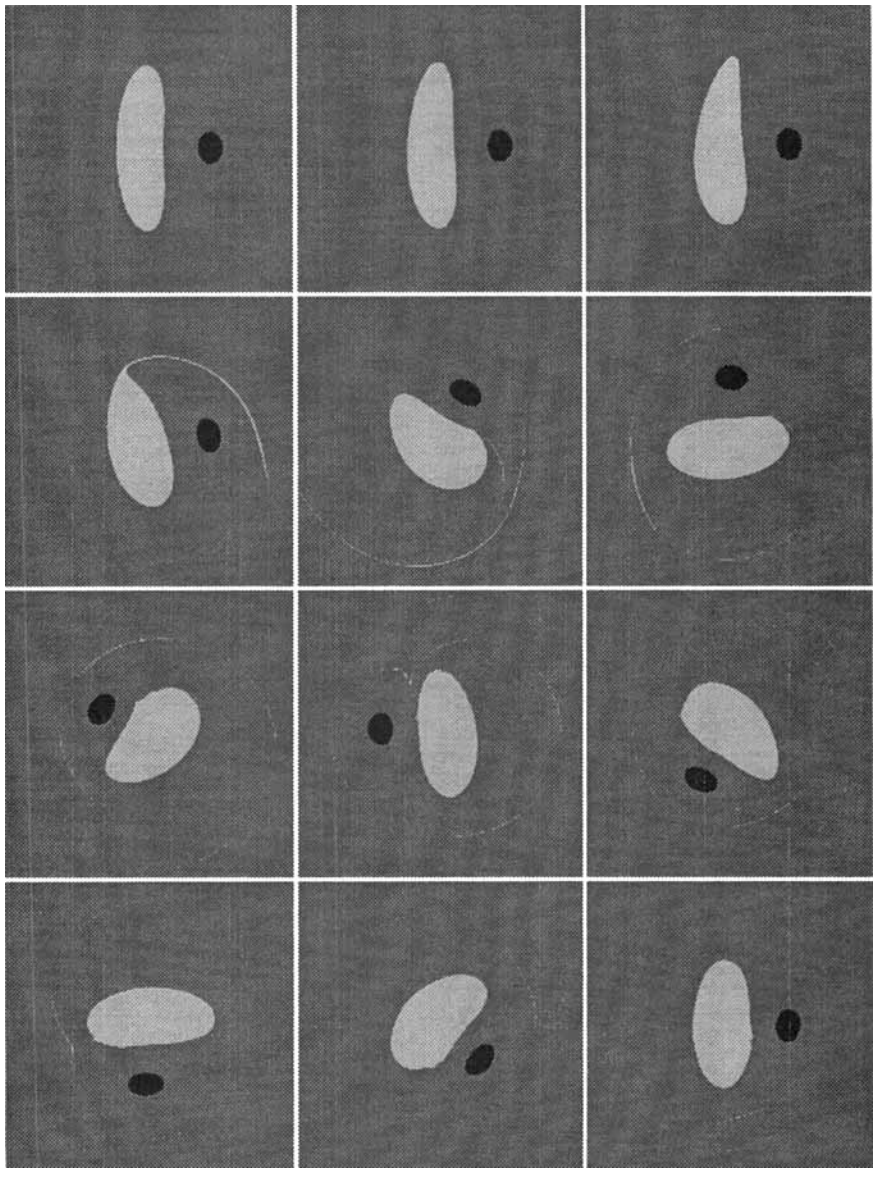

FIGURE 22. Evolution of the marginally unstable opposite-signed equilibrium state for $\alpha = 0.1$.

again increases with initial vortex area ratio, reaching 20% of the total initial area for equal-sized vortices. In (*b*), which shows the initial distance Δ_i between vortex centres, we see that Δ_i depends strongly on α, in contrast to the result for like-signed vortices. One can nevertheless find a simple criterion for the onset of an inelastic interaction: $\Delta_i \lesssim (1.450\text{–}0.464\alpha \pm 0.004)\, L$, where $L \equiv (\mathscr{A}/\pi)^{1/2}$.

In summary, we observe (*a*) that marginally unstable equilibrium states do precipitate inelastic interactions in all cases, (*b*) they begin in the same way via the expulsion of the filament from the more eccentric vortex of the pair (the only exception is for two identical like-signed vortices), and (*c*) they make a rapid transition to a new coherent quasi-steady state, having two vortices in the case of like-signed interactions, or having three vortices in the case of opposite-signed interactions.

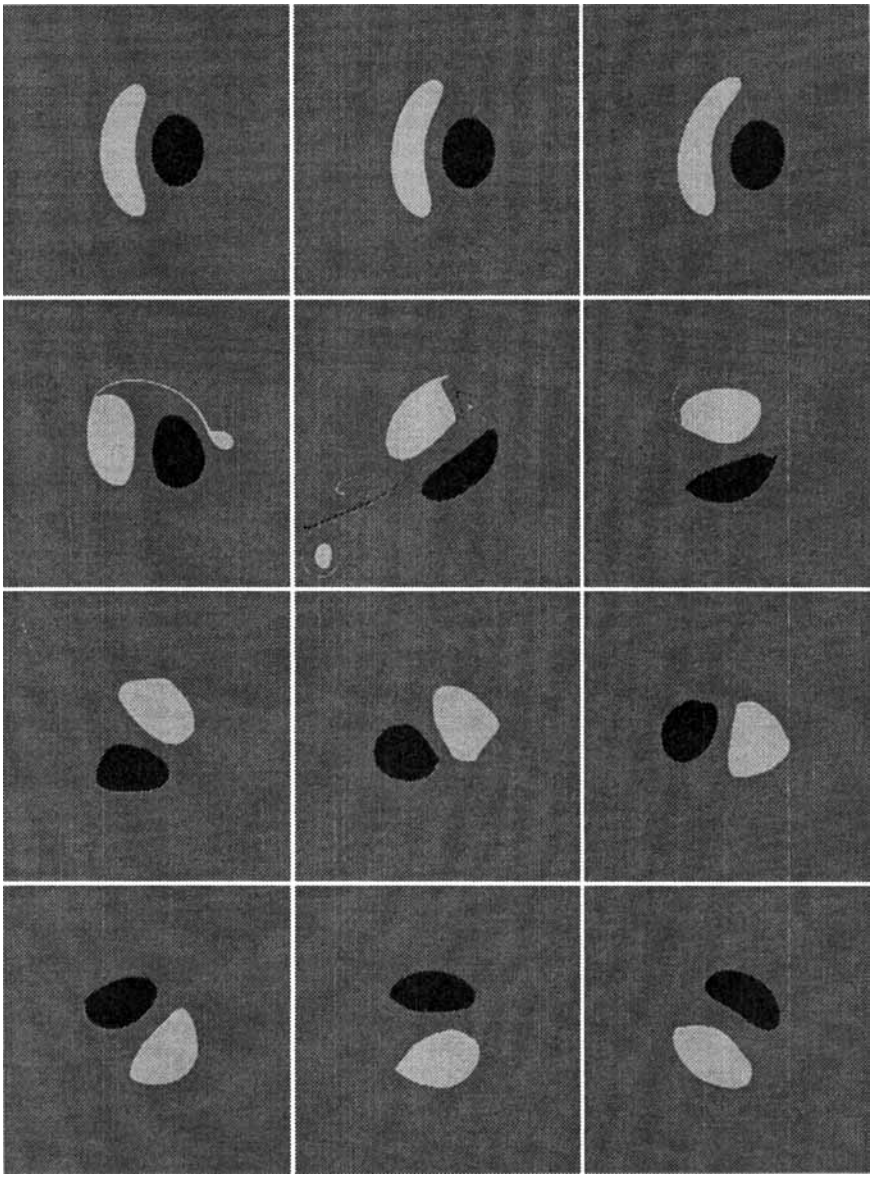

FIGURE 23. As in figure 22, but for $\alpha = 0.7$.

Figures 20 and 25 constitute the major findings of this study. They quantify the outcome of inelastic vortex interactions precipitated by the slow drift of two vortex patches across their marginal stability threshold.

6. Conclusions

The present results have shown that, for generally well-separated vortices which drift only slowly toward or away from each other, vortices tend to assume a near-equilibrium shape functionally dependent on the local ambient strain. When two such vortices move across a certain threshold, a local instability of the two vortices takes place which leads to a short unsteady inelastic interaction. For vortex patches, studied

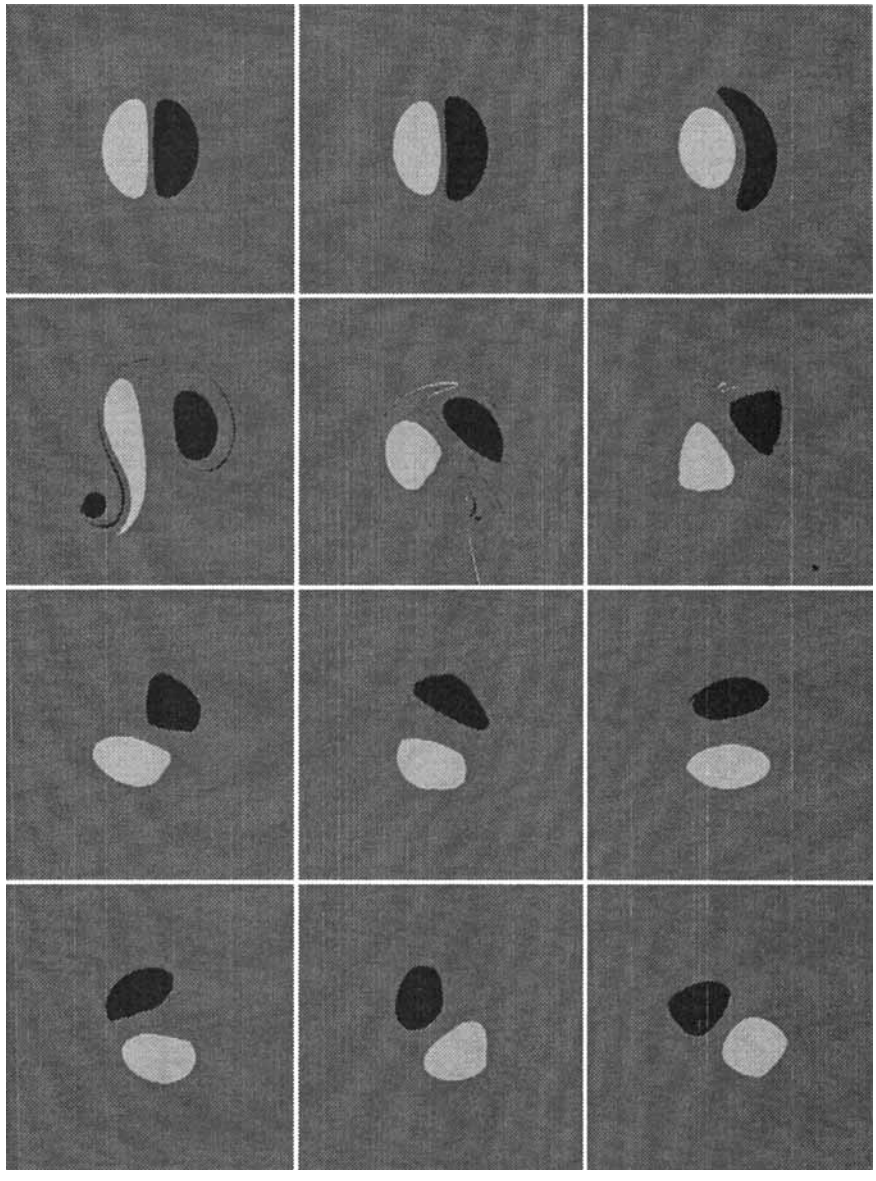

FIGURE 24. As in figure 22, but for $\alpha = 1$.

herein, the first sign of instability is the eruption of a tongue of vorticity from the more eccentric vortex; this has been identified as the mode-3 instability of an elliptical vortex. The tongue then interacts with the other vortex and, in the case of like-signed vortices, if the vortex area ratio exceeds 0.6, the larger vortex incorporates part of this tongue on its periphery and thus grows in size. If the area ratio is less than 0.6, the interaction of the tongue and the larger vortex causes so much filamentation that the larger vortex actually shrinks slightly in size. In the case of opposite-signed vortices, an inelastic interaction always causes the vortices to shrink in size. The coherent state that emerges always consists of two or three quasi-steady vortices. The classical picture of a single product is never observed, and the connection between the inverse energy cascade and inelastic vortex interactions is put into doubt.

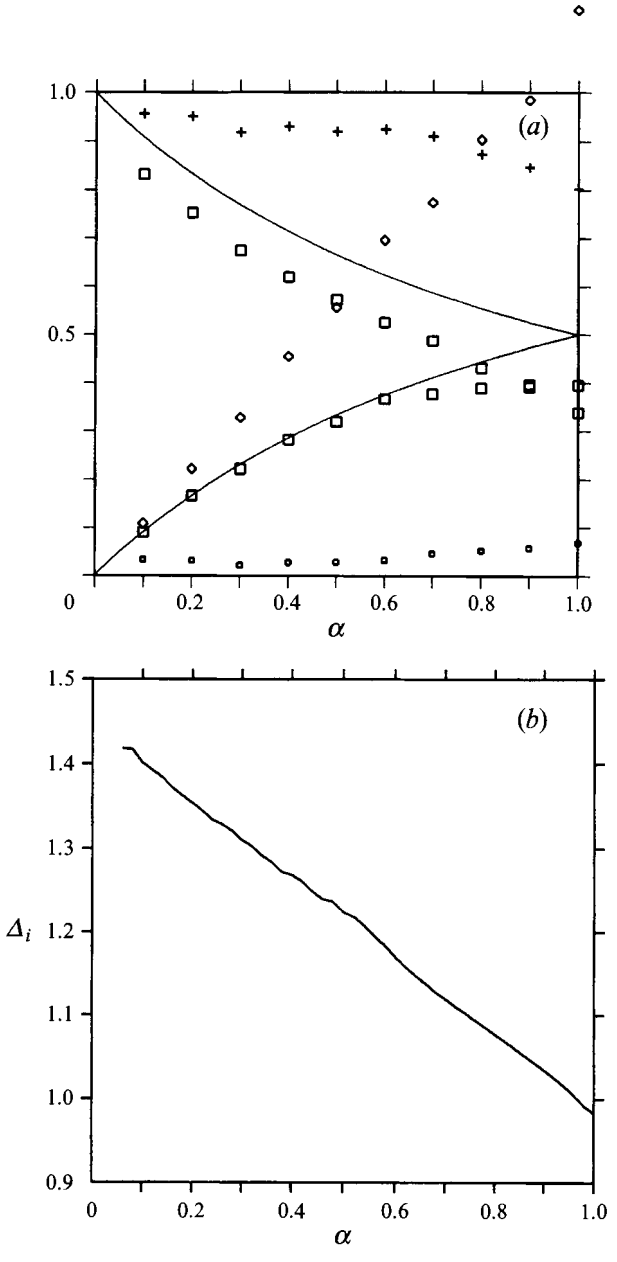

FIGURE 25. (*a*) Transition summary diagram for the inelastic interaction of two opposite-signed vortex patches. As a function of the initial vortex area ratio α, the solid curves give the initial vortex areas divided by π, the squares give the final vortex areas divided by π (the small squares correspond to the tiny vortex which was torn from the larger one initially), the diamonds give the final vortex area ratio (of the two largest vortices), and the crosses give the efficiency (the ratio of the final and initial total area within the principal vortices). (*b*) The distance between vortex centres before the transition. See also table 2.

Are these interactions actually observed in two-dimensional turbulence? Evidence has already been given in the case of like-signed interactions in Dritschel (1993). The fact that there are also opposite-signed inelastic interactions came as a surprise, but a closer examination of vortex behaviour in two-dimensional turbulence reveals that

α_i	Δ_i/L	α_f	Δ_f/L
0.10	1.401	0.1090	1.521
0.20	1.354	0.2214	1.735
0.30	1.310	0.3276	1.879
0.40	1.269	0.4545	2.046
0.50	1.224	0.5566	2.085
0.60	1.171	0.6969	2.169
0.70	1.120	0.7739	2.274
0.80	1.077	0.9038	2.430
0.90	1.035	0.9844	2.498
1.00	0.983	0.8552	2.477

TABLE 2. Opposite-vorticity vortex transition properties. See table 1 for notation

such interactions are apparently as common as their like-signed counterparts – see for example figure 26.

Efforts have been made to construct a simplified model of dilute two-dimensional turbulence based on the present results (in collaboration with N. J. Zabusky and H. B. Yao). However, a vortex-tracking tool recently developed for analysing inelastic interactions in two-dimensional turbulence simulations has revealed a picture considerably more complex than expected. First, inelastic interactions occur between *at least* three vortices typically, and, secondly they result in vortex structures which are clearly the product of the locally complex time-dependent straining field of all the vortices involved (see Dritschel & Zabusky 1995). While the ingoing states often evolve adiabatically, and the initial stage of the inelastic interaction is similar to that described in the present paper, the final stages depend, and therefore so do the resulting vortices, on all the nearby surrounding vortices. That is, the local, externally produced straining field cannot be neglected in the final stages of any interaction. These findings appear to thwart any chance to construct a simplified model of nearly inviscid two-dimensional turbulence at the vortex level. We propose (in Dritschel & Zabusky 1995), alternatively, an intermediate-level model – the Hybrid Elliptical-Contour (HEC) model – which uses an elliptical representation for vortices experiencing weak levels of external straining, and which otherwise uses a contour representation. In this model, inelastic interactions are carried out using the full contour surgery algorithm. We believe that this model is the simplest asymptotic model for nearly inviscid two-dimensional turbulence.

A theory for two-dimensional turbulence appears more distant than ever, if one expects such a theory at the vortex level. The difficulty, as just discussed, is parameterizing the result of an inelastic vortex interaction. There simply appears to be too many parameters to make this feasible – or intelligible. What the present work has shown is that the individual vortex interactions in two-dimensional turbulence exhibit common evolutionary characteristics. Whether or not this implies some kind of universality for the collective behaviour of a multitude of vortices – for two-dimensional turbulence – remains an intriguing question.

This paper has focused on the simplest case of vortex patches having equal vorticity magnitude. One might wonder about cases in which the vorticity is not uniform and varies from vortex to vortex. When the vorticity is not uniform, the stripping process efficiently removes a vortex's peripheral vorticity up to a level dependent on the amount of strain experienced by the vortex (Legras & Dritschel 1993 and references therein). Inelastic vortex interactions are characterized by relatively strong levels of

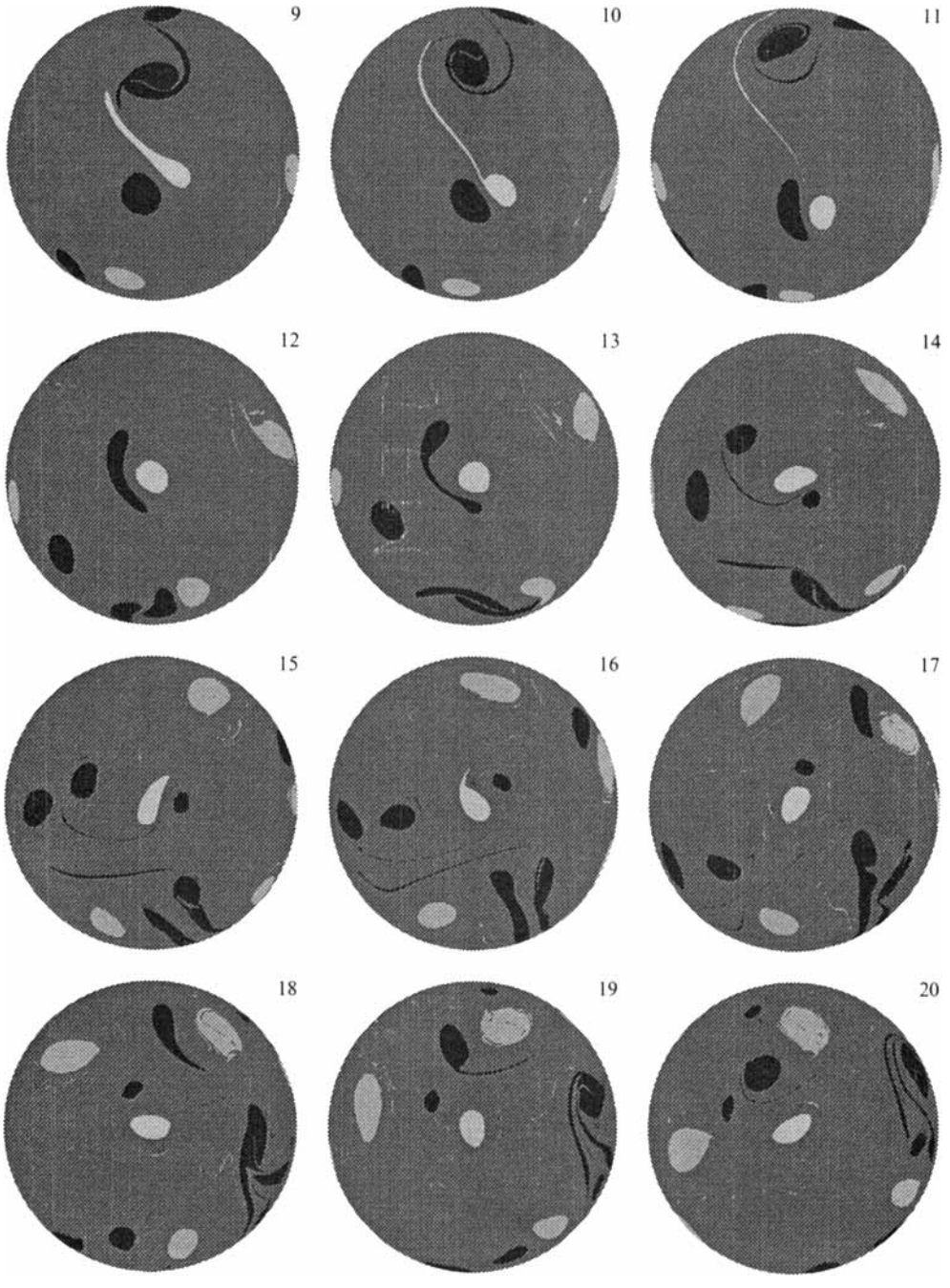

FIGURE 26. Selected times from a calculation of two-dimensional turbulence on a unit sphere showing an inelastic interaction between opposite-signed vortices. All vortices are patches having equal vorticity magnitude, and the time (indicated to the upper-right of each frame) is in units of a vortex rotation period. Initially 10% of the domain is occupied by 10 positive and 10 negative equal-sized vortices. Times 9 and 10 show the formation of a mismatched dipole, times 11–16 show the subsequent instability of this dipole, and times 17–20 show the separation of the dipole by surrounding vortices. The calculation was performed with contour surgery using the numerical parameters $\Delta t = 0.05$, $\mu = 0.15$ and $\delta = 0.0016$.

strain and produce vortices with moderate edge vorticity values (Waugh 1992; Dritschel 1993; Mariotti, Legras & Dritschel 1994; Yao, Dritschel & Zabusky 1995). In the absence of forcing and dissipation that would smear out vortex edges, it stands to reason that a vortex would become progressively more patch-like after successive inelastic interactions, simply because its weaker edge vorticity is more susceptible to being stripped away and 'lost' to filaments than the high-level vorticity found near the vortex centre. For the same reason, in a flow with vortices of varying peak vorticity, the vortices with the highest peak vorticity would tend to eliminate the vortices having significantly lower peak vorticity. Hence, though the vortex patch idealizes the likely parabolic-topped shape (Legras & Dritschel 1993) of vortices after many inelastic interactions, it is not an unreasonable approximation, and, of course, it is simple. It is the first step.

Finally, it is worth asking in future research how the present results may apply to the more general layerwise-two-dimensional flows characteristic of the oceans and the atmosphere. As a start in this direction, a simple change of the Green function from $\log r$ to $-K_0(r/L)$ or a combination of the two functions as in multi-layer quasi-geostrophic flow (Dritschel & Saravanan 1994) does not appear so significant as to qualitatively alter the present results. A quantitative study is nevertheless merited and may lead to a deeper understanding of the vortex interaction process in geophysical fluid dynamics.

Support for this research has come from the UK Natural Environment Research Council. Additional support was provided by the Innovative Science and Technology Program through grant number N00014-92-J-2009 administered by the US Naval Research Laboratory, by the Isaac Newton Trust, by NATO, and by the European Community.

Appendix A. The construction of an optimal instantaneous co-rotating reference frame

Details are given here for how the rotating-frame streamfunction was computed in the calculation illustrated in figure 1. In general, the object is to determine, in some optimal sense, the rotating frame of reference in which contours of vorticity and of streamfunction are most closely aligned (perfect alignment implies the flow is in equilibrium). The streamfunction in this rotating frame is given by

$$\psi' = \psi - \tfrac{1}{2}\Omega |\boldsymbol{x}|^2, \tag{A 1}$$

where Ω is the rotation rate. In general, Ω is a function of time. Here, ψ is the streamfunction in the original frame of reference (i.e. $\nabla^2\psi = \omega$). Ω is determined, formally, by minimizing

$$F(\Omega) \equiv \int\int \mathrm{d}x\,\mathrm{d}y(\partial\omega'/\partial t)^2/|\nabla\omega|, \tag{A 2}$$

where $\partial\omega'/\partial t = -J(\psi', \omega) = -\boldsymbol{u}' \cdot \nabla\omega$, and $\boldsymbol{u}'$ is the velocity in the rotating frame:

$$\boldsymbol{u}' = \boldsymbol{u} + \Omega\{y, -x\}. \tag{A 3}$$

Letting $\nabla\omega \equiv |\nabla\omega|\,\hat{\boldsymbol{n}}$ define the unit normal vector $\hat{\boldsymbol{n}}$ for any vorticity contour (ω = constant), (A 2) can be re-written as

$$F(\Omega) = \int\int \mathrm{d}x\,\mathrm{d}y\,|\nabla\omega|\,(\boldsymbol{u}' \cdot \hat{\boldsymbol{n}})^2 \tag{A 4}$$

revealing why $1/|\nabla\omega|$ is used in the integrand of (A 2): only with this weight does (A 2) have a meaningful limit for a piecewise-constant distribution of vorticity; this limit is given by

$$F(\Omega) = \sum_k |\tilde{\omega}_k| \oint_{\mathscr{C}_k} \mathrm{d}s(\boldsymbol{u}' \cdot \hat{\boldsymbol{n}})^2, \tag{A 5}$$

where $|\tilde{\omega}_k|$ is the magnitude of the vorticity jump across $\mathscr{C}_k$ and s is arclength.

In this paper, the distribution of vorticity is piecewise constant, so (A 5) is used. Minimizing F with respect to Ω (setting $\partial F/\partial\Omega = 0$) leads to the following simple expression for Ω:

$$\Omega = \frac{\sum_k |\tilde{\omega}_k| \oint_{\mathscr{C}_k} \mathrm{d}s(\boldsymbol{x} \cdot \hat{\boldsymbol{t}})\,(\boldsymbol{u} \cdot \hat{\boldsymbol{n}})}{\sum_k |\tilde{\omega}_k| \oint_{\mathscr{C}_k} \mathrm{d}s(\boldsymbol{x} \cdot \hat{\boldsymbol{t}})^2}, \tag{A 6}$$

where $\hat{\boldsymbol{t}}$ is the unit tangent vector, i.e. $\hat{\boldsymbol{t}} = \{t_x, t_y\} = \{n_y, -n_x\}$.

The quantity F measures, quantitatively, how closely the ω and ψ contours are matched and hence how steady the instantaneous flow appears in this frame of reference. Dividing F by the denominator of (A 6) multiplied by the peak vorticity magnitude ω_p squared gives a dimensionless measure of the degree of unsteadiness, the normalized squared variance ϵ^2:

$$\epsilon^2(t) \equiv \frac{\sum_k |\tilde{\omega}_k| \oint_{\mathscr{C}_k} \mathrm{d}s(\boldsymbol{u}' \cdot \hat{\boldsymbol{n}})^2}{\omega_p^2 \sum_k |\tilde{\omega}_k| \oint_{\mathscr{C}_k} \mathrm{d}s(\boldsymbol{x} \cdot \hat{\boldsymbol{t}})^2}, \tag{A 7}$$

whose continuous form reads

$$\epsilon^2(t) \equiv \frac{\int\int \mathrm{d}x\,\mathrm{d}y\,|\nabla\omega|\,(\boldsymbol{u}' \cdot \hat{\boldsymbol{n}})^2}{\omega_p^2 \int\int \mathrm{d}x\,\mathrm{d}y\,|\nabla\omega|\,(\boldsymbol{x} \cdot \hat{\boldsymbol{t}})^2}. \tag{A 8}$$

Other procedures exist for constructing an 'optimal' rotating frame of reference (e.g. see Melander, McWilliams & Zabusky 1987), but the one presented here seems the easiest to implement in practice. Furthermore, this idea can be simply extended to determine, perhaps in addition to the background rotation Ω, the mean translation rate of the vortex system as well as higher-order characteristics of the local flow field (e.g. the background strain). This diagnostic may thus prove useful for examining vortex interactions in two-dimensional turbulence.

Appendix B. The linear stability method

The method described next was first used by Dritschel & Legras (1991) to determine the stability of nested elliptical-like distributions of vorticity. However, the method itself has remained unpublished (it differs substantially from the method originally presented by Dritschel 1985). Here, we give a brief outline of this 'new' method.

Let a subscript e denote equilibrium quantities (apart from their basic properties, such as their rotation rate Ω). Quantities without a subscript refer to the disturbed

flow. The basic idea is to represent a disturbance to any vorticity contour of the equilibrium state as follows:

$$\boldsymbol{x}(\theta, t) = \boldsymbol{x}_e(\theta) + \eta(\theta, t) \frac{\{\mathrm{d}y_e/\mathrm{d}\theta, -\mathrm{d}x_e/\mathrm{d}\theta\}}{(\mathrm{d}x_e/\mathrm{d}\theta)^2 + (\mathrm{d}y_e/\mathrm{d}\theta)^2}, \tag{B 1}$$

i.e. as a normal displacement (we consider, thus, only perturbations that could arise under the action of a weak irrotational external field). Here, the correction to $\boldsymbol{x}_e$ is considered small compared with $\boldsymbol{x}_e$ itself so that we may linearize the equations of motion keeping terms only to first order in η, the 'disturbance function'.

The variable θ can be any parametrization of the vorticity contour, but there is a special parametrization that leads to particular simplicity, namely θ being proportional to the travel time for a fluid particle to go from some fixed location along the equilibrium vorticity contour to some other location (we choose the normalization constant so that $\theta = 2\pi$ for a complete circuit of the contour). If we denote the frequency with which particles circuit the kth equilibrium contour by Ω_{ek}, then the disturbance function of the kth contour $\eta_k(\theta_k, t)$ evolves according to

$$\frac{\partial \eta_k}{\partial t} + \Omega_{ek} \frac{\partial \eta_k}{\partial \theta_k} = \frac{\partial F_k}{\partial \theta_k}, \tag{B 2a}$$

where

$$F_k(\theta_k) \equiv -\sum_{j=1}^{n} \frac{\tilde{\omega}_j}{2\pi} \int_0^{2\pi} \eta_j(\theta_j, t) \log |\boldsymbol{x}_{ek}(\theta_k) - \boldsymbol{x}_{ej}(\theta_j)| \, \mathrm{d}\theta_j, \tag{B 2b}$$

and where n is the total number of contours (two in the problem considered in this paper) and $\tilde{\omega}_j$ is the inward vorticity jump across the jth contour (± 1 for all the contours considered here).

There are several remarkable features of this equation. First, the overall rotation rate Ω does not appear explicitly (it does enter the calculation of the parametrization, θ). Secondly, the eigenfunctions for an elliptical vortex patch are simply $(A_m \cos m\theta + B_m \sin m\theta)\mathrm{e}^{\sigma t}$, $m = 1, 2, \ldots$, i.e. there is no mode coupling (Love 1893; Dritschel 1990). Third, the equation remains unchanged in the presence of an external straining field. And fourth, the equation can be used to test the stability of more general two-dimensional flows by replacing $(2\pi)^{-1} \log r$ in (3b) by the appropriate Green function G (under the weak restriction that G depends only on the coordinate differences between points).

In general, the mode decoupling that occurs for the elliptical vortex patch does not extend to other equilibrium states. We therefore represent the disturbance function η_k on each contour by a finite sum of cosines and sines, up to order $m = M$. By inserting this sum into (2), we arrive at a matrix eigen-problem for the eigenvalue σ and the mode amplitudes A_{mk} and B_{mk} (where k refers to the contour index). The matrix order is $2Mn \times 2Mn$.

In a previous work (Dritschel 1985), the disturbance was not allowed to modify the angular impulse J. The argument forwarded then (and originally by Thomson 1883 in his linear stability analysis of a system of co-rotating point vortices) was that any change to the angular impulse would require an infinite amount of energy to bring about, and hence was not realizable. In the present work, however, we imagine there to be a weak external field (e.g. due to distant, but not infinitely distant, vortices) capable of pushing the vortices together and, hence, capable of modifying their angular impulse. Thus, we do not impose this constraint here. On the other hand, we do impose the constraint that the area of each contour remains unchanged. Irrotationally

produced disturbances cannot modify the area of vorticity contours. This constraint is automatically imposed by the choice of disturbance representation taken in (B 1).

The numerical procedures involved are described only briefly. Cubic-spline interpolation and two-point Gaussian quadrature are used to set up the parameterization θ and to perform the integral in (B 2b), using all 398 nodes per contour of the equilibrium states. Special care is taken to avoid integrating through the logarithmic singularity in (B 2b) by adding and subtracting the term $\frac{1}{2}\log(1-\cos(\theta_k-\theta_j))$ from the logarithm in the integrand. The integral over this term can be performed analytically, leaving one to compute only the integral of the non-singular difference of two singular functions. The numerical package NAG is used to calculate the eigenvalues (σ) and eigenvectors (A_{mk}, B_{mk}, $m = 1, 2, \ldots, M$, $k = 1, 2$). $M = 50$ modes are used in the results presented. Some selected states were analysed using $M = 100$ modes, and the eigenvalues were found to shift by less than 0.0001 except very close to the marginal stability boundary, where approximately ten times greater error was observed.

REFERENCES

AREF, H. 1979 Motion of three vortices. *Phys. Fluids* **22**, 393–400.

BENZI, R., BRISCOLINI, M., COLELLA, M. & SANTANGELO, P. 1992 A simple point vortex model for two-dimensional decaying turbulence. *Phys. Fluids* A **4**, 1036–1039.

BRACHET, M. E., MENEGUZZI, M., POLITANO, H. & SULEM, P. L. 1988 The dynamics of freely decaying two-dimensional turbulence. *J. Fluid Mech.* **194**, 333–349.

CARNEVALE, G. F., MCWILLIAMS, J. C., POMEAU, Y., WEISS, J. B. & YOUNG, W. R. 1991 Evolution of vortex statistics in two-dimensional turbulence. *Phys. Rev. Lett.* **66**, 2735–2737.

DRITSCHEL, D. G. 1985 The stability and energetics of corotating uniform vortices. *J. Fluid Mech.* **157**, 95–134.

DRITSCHEL, D. G. 1986 The nonlinear evolution of rotating configurations of uniform vorticity. *J. Fluid Mech.* **172**, 157–182.

DRITSCHEL, D. G. 1988*a* Contour surgery: a topological reconnection scheme for extended integrations using contour dynamics. *J. Comput. Phys.* **77**, 240–266.

DRITSCHEL, D. G. 1988*b* The repeated filamentation of two-dimensional vorticity interfaces. *J. Fluid Mech.* **194**, 511–547.

DRITSCHEL, D. G. 1989*a* Contour dynamics and contour surgery: numerical algorithms for extended, high-resolution modelling of vortex dynamics in two-dimensional, inviscid, incompressible flows. *Comput. Phys. Rep.* **10**, 77–146.

DRITSCHEL, D. G. 1989*b* Strain-induced vortex stripping. In *Mathematical Aspects of Vortex Dynamics* (ed. R. E. Caflisch), pp. 107–119. SIAM.

DRITSCHEL, D. G. 1989*c* On the stabilization of a two-dimensional vortex strip by adverse shear. *J. Fluid Mech.* **206**, 193–221.

DRITSCHEL, D. G. 1990 The stability of elliptical vortices in an external straining flow. *J. Fluid Mech.* **210**, 223–261.

DRITSCHEL, D. G. 1993 Vortex properties of two-dimensional turbulence. *Phys. Fluids* A **5**, 984–997.

DRITSCHEL, D. G., HAYNES, P. H., JUCKES, M. N. & SHEPHERD, T. G. 1991 The stability of a two-dimensional vorticity filament under uniform strain. *J. Fluid Mech.* **230**, 647–665.

DRITSCHEL, D. G. & LEGRAS, B. 1991 The elliptical model of two-dimensional vortex dynamics. Part II: disturbance equations. *Phys. Fluids* A **3**, 855–868.

DRITSCHEL, D. G. & SARAVANAN, R. 1994 Three-dimensional quasi-geostrophic contour dynamics, with an application to stratospheric vortex dynamics. *Q. J. R. Met. Soc.* **120**, 1267–1297.

DRITSCHEL, D. G. & WAUGH, D. W. 1992 Quantification of the inelastic interaction of two asymmetric vortices in two-dimensional vortex dynamics. *Phys. Fluids* A **4**, 1737–1744.

DRITSCHEL, D. G. & ZABUSKY, N. J. 1995 Toward a reduced model for nearly-inviscid unforced two-dimensional turbulence. *Phys. Fluids* (submitted).

GRÖBLI, W. 1877 *Specielle Probleme über die Bewegung geradliniger paralleler Wirbelfäden.* Zürich: Zürcher und Furrer. (Also published in *Vierteljahrsschrift der Naturforschenden Gesellschaft in Zürich*, vol. 22, pp. 37–81; 129–165.)

KAMM, R. 1987 PhD thesis, California Institute of Technology.

LEGRAS, B. & DRITSCHEL, D. G. 1993 Vortex stripping and the generation of high vorticity gradients in two-dimensional flows. *Appl. Sci. Res.* **51**, 445–455.

LOVE, A. E. H. 1893 On the stability of certain vortex motions. *Proc. Lond. Math. Soc.* **35**, 18.

MARIOTTI, A., LEGRAS, B. & DRITSCHEL, D. G. 1994 Vortex stripping and erosion of coherent structures in two-dimensional flows. *Phys. Fluids* **6**, 3954–3962.

MCWILLIAMS, J. C. 1990 The vortices of two-dimensional turbulence. *J. Fluid Mech.* **219**, 361–385.

MELANDER, M. V., MCWILLIAMS, J. C. & ZABUSKY, N. J. 1987 Axisymmetrization and vorticity gradient intensification of an isolated two-dimensional vortex through filamentation. *J. Fluid Mech.* **178**, 137–159.

OVERMAN, E. A. II 1986 Steady-state solutions of the Euler equations in two dimensions. II. Local Analysis of limiting V-states. *SIAM J. Appl. Maths.* **46**, 765–800.

PIERREHUMBERT, R. T. 1980 A family of steady, translating vortex pairs with distributed vorticity. *J. Fluid Mech.* **99**, 129–144.

POLVANI, L. M. & DRITSCHEL, D. G. 1993 Nonlinear Vortex dynamics on the surface of the sphere: Equilibria and their stability. *J. Fluid Mech.* **255**, 35–64.

SAFFMAN, P. G. 1992 *Vortex Dynamics.* Cambridge University Press.

SANTANGELO, P., BENZI, R. & LEGRAS, B. 1989 The generation of vortices in high-resolution, two-dimensional decaying turbulence and the influence of initial conditions on the breaking of self-similarity. *Phys. Fluids* A **1**, 1027–1034.

THOMSON, J. J. 1883 *A Treatise on the Motion of Vortex Rings*, pp. 94–108. Macmillan.

WAUGH, D. W. 1992 The efficiency of symmetric vortex merger. *Phys. Fluids* A **4**, 1745–1758.

YAO, H. B., DRITSCHEL, D. G. & ZABUSKY, N. J. 1995 High-gradient phenomena in 2D vortex interactions. *Phys. Fluids* **7**, 539–548.

ZABUSKY, N. J., HUGHES, M. H. & ROBERTS, K. V. 1979 Contour dynamics for the Euler equations in two dimensions. *J. Comput. Phys.* **30**, 96–106.